T.C.
REPUBLIC OF TURKEY
HACETTEPE UNIVERSITY
GRADUATE SCHOOL OF HEALTH SCIENCES

OPTICAL MONITORING OF CEREBRAL BLOOD FLOW AND METABOLISM DURING CAROTID ENDARTERECTOMY

Kutlu KAYA, M.S.

Program of Physiology
DOCTOR OF PHILOSOPHY DISSERTATION

ANKARA
2022

T.C.
REPUBLIC OF TURKEY
HACETTEPE UNIVERSITY
GRADUATE SCHOOL OF HEALTH SCIENCES

OPTICAL MONITORING OF CEREBRAL BLOOD FLOW AND METABOLISM DURING CAROTID ENDARTERECTOMY

Kutlu KAYA, M.S.

Program of Physiology
DOCTOR OF PHILOSOPHY DISSERTATION

SUPERVISOR
Prof. Dr. Ethem GELİR

CO-SUPERVISOR
Prof. Dr. Maria Angela FRANCESCHINI

ANKARA
2022

HACETTEPE UNIVERSITY

GRADUATE SCHOOL OF HEALTH SCIENCES

Optical Monitoring of Cerebral Blood Flow and Metabolism During Carotid Endarterectomy

Kutlu KAYA, M.S.

Supervisor: Prof. Dr. Ethem GELİR

Co-supervisor: Prof. Dr. Maria Angela FRANCESCHINI

This thesis study has been approved and accepted as a Ph.D. dissertation in the "Physiology Program" by the assessment committee, whose members are listed below, on September 23, 2022.

Chairman of the Committee	*Prof. Dr. Metehan ÇİÇEK* *Ankara University*
Member:	*Assoc. Prof. Dr. Bilge PEHLİVANOĞLU* *Hacettepe University*
Member:	*Assoc. Prof. Dr. Okan ARIHAN* *Hacettepe University*
Member:	*Assist. Prof. Dr. Hasan Onur KELEŞ* *Ankara University*
Member:	*Assist. Prof. Dr. Murat Perit ÇAKIR* *Middle East Technical University*

This dissertation has been approved by the above committee in conformity to the related issues of Hacettepe University Graduate Education and Examination Regulation.

Prof. Müge YEMİŞCİ ÖZKAN, MD, PhD

Director

YAYINLAMA VE FİKRİ MÜLKİYET HAKLARI BEYANI

Enstitü tarafından onaylanan lisansüstü tezimin/raporumun tamamını veya herhangi bir kısmını, basılı (kağıt) ve elektronik formatta arşivleme ve aşağıda verilen koşullarla kullanıma açma iznini Hacettepe Üniversitesine verdiğimi bildiririm. Bu izinle Üniversiteye verilen kullanım hakları dışındaki tüm fikri mülkiyet haklarım bende kalacak, tezimin tamamının ya da bir bölümünün gelecekteki çalışmalarda (makale, kitap, lisans ve patent vb.) kullanım hakları bana ait olacaktır.

Tezin kendi orijinal çalışmam olduğunu, başkalarının haklarını ihlal etmediğimi ve tezimin tek yetkili sahibi olduğumu beyan ve taahhüt ederim. Tezimde yer alan telif hakkı bulunan ve sahiplerinden yazılı izin alınarak kullanılması zorunlu metinlerin yazılı izin alınarak kullandığımı ve istenildiğinde suretlerini Üniversiteye teslim etmeyi taahhüt ederim.

Yükseköğretim Kurulu tarafından yayınlanan ***"Lisansüstü Tezlerin Elektronik Ortamda Toplanması, Düzenlenmesi ve Erişime Açılmasına İlişkin Yönerge"*** kapsamında tezim aşağıda belirtilen koşullar haricince YÖK Ulusal Tez Merkezi / H.Ü. Kütüphaneleri Açık Erişim Sisteminde erişime açılır.

- Enstitü / Fakülte yönetim kurulu kararı ile tezimin erişime açılması mezuniyet tarihimden itibaren 2 yıl ertelenmiştir. (1)
- Enstitü / Fakülte yönetim kurulunun gerekçeli kararı ile tezimin erişime açılması mezuniyet tarihimden itibaren 6 ay ertelenmiştir. (2)
- Tezimle ilgili gizlilik kararı verilmiştir. (3)

23/09/2022

Arş. Gör. Kutlu KAYA

i

[i] *"Lisansüstü Tezlerin Elektronik Ortamda Toplanması, Düzenlenmesi ve Erişime Açılmasına İlişkin Yönerge"*

*(1) Madde 6. 1. Lisansüstü tezle ilgili patent başvurusu yapılması veya patent alma sürecinin devam etmesi durumunda, tez **danışmanının** önerisi ve **enstitü anabilim dalının** uygun görüşü üzerine **enstitü** veya **fakülte yönetim kurulu** iki yıl süre ile tezin erişime açılmasının ertelenmesine karar verebilir.*

*(2) Madde 6. 2. Yeni teknik, materyal ve metotların kullanıldığı, henüz makaleye dönüşmemiş veya patent gibi yöntemlerle korunmamış ve internetten paylaşılması durumunda 3. şahıslara veya kurumlara haksız kazanç imkanı oluşturabilecek bilgi ve bulguları içeren tezler hakkında tez **danışmanının** önerisi ve **enstitü anabilim dalının** uygun görüşü üzerine **enstitü** veya **fakülte yönetim kurulunun** gerekçeli kararı ile altı ayı aşmamak üzere tezin erişime açılması engellenebilir.*

*(3) Madde 7. 1. Ulusal çıkarları veya güvenliği ilgilendiren, emniyet, istihbarat, savunma ve güvenlik, sağlık vb. konulara ilişkin lisansüstü tezlerle ilgili gizlilik kararı, **tezin yapıldığı kurum** tarafından verilir *. Kurum ve kuruluşlarla yapılan işbirliği protokolü çerçevesinde hazırlanan lisansüstü tezlere ilişkin gizlilik kararı ise, **ilgili kurum ve kuruluşun önerisi** ile **enstitü** veya **fakültenin** uygun görüşü üzerine **üniversite yönetim kurulu** tarafından verilir. Gizlilik kararı verilen tezler Yükseköğretim Kuruluna bildirilir.*
Madde 7.2. Gizlilik kararı verilen tezler gizlilik süresince enstitü veya fakülte tarafından gizlilik kuralları çerçevesinde muhafaza edilir, gizlilik kararının kaldırılması halinde Tez Otomasyon Sistemine yüklenir

****** Tez **danışmanının** önerisi ve **enstitü anabilim dalının** uygun görüşü üzerine **enstitü** veya **fakülte yönetim kurulu tarafından karar verilir.***

ETHICAL DECLARATION

In this dissertation study, I declare that all the information and documents have been obtained based on the academic rules, and all audio-visual and written information and results have been presented according to the rules of scientific ethics. I did not do any distortion in the data set. In the case of using other works, related studies have been fully cited in accordance with the scientific standards. I also declare that my thesis study is original except for cited references. It was produced by myself in consultation with my co-supervisor Prof. Dr. Maria Angela Franceschini (Massachusetts General Hospital and Harvard Medical School) and written according to the rules of thesis writing of Hacettepe University Graduate School of Health Sciences.

Kutlu KAYA, M.S.

To my precious wife and daughter…

ACKNOWLEDGEMENTS

The journey of my doctoral studies started in Ankara, then moved to Boston. When I look back, I am so grateful for every second of this journey. There are many people I would like to thank for their contribution, friendship, guidance, and mentorship. First, I would like to share my sincere appreciation to my advisor Dr. Ethem Gelir for his friendship, encouragement, perseverance, and endless support. I am also grateful to each faculty member and assistant at Hacettepe Physiology for sharing enthusiasm for science and excellence in education and tutoring. The time I spent in Hacettepe Physiology was fruitful and priceless in so many ways because of them. I wish to thank my thesis examining committee members Drs. Kader Karlı Oğuz and Metehan Çiçek for their rigorous contributions. I would like to express my deepest gratitude to my dissertation advisor Dr. Maria Angela Franceschini. The opportunity of conducting research in Franceschini's lab with other valuable members of Optics at Athinoula A. Martinos Center for Biomedical Imaging was a great privilege. I am happy to have been able to work under the guidance of a leading scientist in the field of biomedical optics. The time I spent in Optics at Martinos Center fueled me further to conduct intellectually stimulating research. I wish to thank all of my friends and colleagues for their support in my scientific and personal life. I am really grateful to Drs. Stefan Carp, John Sunwoo, Felipe Oriheula-Espina, Marco Renna, Mitchell Robinson, and Alexander I. Zavriyev, Allen Alfadhel, Alyssa Martin, Kuan-Cheng 'Tony' Wu, Zachary Starkweather, and other members of the Optics group at Martinos Center. I would also like to thank Drs. Eric T. Pierce, Mirela V. Simon, and Glenn M. LaMuraglia for assistance in the clinical side of my dissertation.

Finally, I am grateful to my family for their support. However, beyond everything, I am enormously grateful to my wife, soon-to-be-doctor Nihan Balşık Kaya, not just because of her never-ending and unrequited support in my life, but also for giving me the most valuable title in the world, Dad! Fatherhood is probably the purest and most beautiful feeling anyone can feel. Every day, I wake up with my lovely daughter Evrim Nil Kaya and this brings out the best aspects of myself even more.

ÖZET

Kaya K., Karotis Endarterektomi Sırasında Serebral Kan Akımı ve Metabolizmasının Optik İzlenmesi, Hacettepe Üniversitesi Sağlık Bilimleri Enstitüsü Fizyoloji Programı Doktora Tezi, Ankara, 2022. Karotis endarterektomi (KEA), karotis bifurkasyondaki plak kaynaklı embolik inme riski altında olan hastalarda bu plağı ortadan kaldırmak için yapılan cerrahi bir operasyondur. Cerrahi alanda kan akımını durdurmak için KEA karotis arterlerin (ortak, iç ve dış) çapraz klemplenmesini gerektirir, bu da ipsilateral yarımkürede hemodinamik bir zorluğa ve emboli riskine neden olur. Bu nedenle, serebral hemodinami veya elektrofizyoloji farklı nörogörüntüleme teknikleri ile intraoperatif izlenir (örn., yakın kızılötesi spektroskopisi (NIRS), elektroensefalogram (EEG), somatosensoriyel uyarılmış potansiyeller, karotis güdük basıncı ve transkraniyal Doppler ultrason). KEA sırasında EEG yaygın olarak kullanılmakta ve güvenilir bir izleme tekniği olarak görülmesine rağmen, serebral kan akımının (SKA) vekil bir ölçümüdür. Ek olarak, farklı anestezi uygulamaları EEG dalgalarını baskılayabilir ve yeterli SKA tespitini zorlaştırabilir. Ayrıca, KEA sırasında SKA'nın izlenmesi için altın bir standart bulunmamaktadır. Bu nedenle, KEA hastalarında birleşik diffüz korelasyon spektroskopisi (DCS) ve NIRS sistemi ile SKA indeksi (SKA_i) ve serebral metabolizmadaki değişiklikleri araştırmayı amaçladık. Güvenilir bir EEG spektral analiz yöntemi olan desenkronizasyon fonksiyonunu kullanarak yirmi üç KEA hastasında EEG güç spektrumlarındaki değişiklikleri serebral hemodinami ile karşılaştırdık. Ayrıca, klemp sonuncu oluşan elektrofizyolojik ve nörovasküler değişiklikleri göstermek için desenkronizasyon fonksiyonlarında farklı indüksiyon anestezilerini değerlendirdik. Son olarak, hemisferik farklılıkları yakalamak için varyasyon katsayısını ölçerek SKA_i ve EEG güç spektrumları içindeki değişkenliği değerlendirdik. Birleşik bir DCS-NIRS sistemi, KEA sırasında elektrofizyolojiyi tamamlayıcı serebral hemodinami değerlendirmesi sunabilir. DCS-NIRS birleşik sistemi ile intraoperatif nörogörüntüleme klemple indüklenen serebral hipoperfüzyonun izlenmesine ve yatan hasta bakımında akut yönetim değişikliklerinin yapılmasına yardımcı olacaktır (örn., arteriyal şant). Beynin elektrofizyolojik ve nörovasküler durumunun değerlendirilmesi, hipoperfüzyon ve hipoksi gibi istenmeyen olayları ve serebral iskemiyi önleyebilir ve kişiselleştirilmiş perfüzyon stratejilerinin belirlenmesine izin verebilir.

Anahtar Kelimeler: İntraoperatif nörogörüntüleme, karotis endarterektomi, diffüz korelasyon spektroskopisi, beyin kan akımı, yakın kızılötesi spektroskopi, anestezi

ABSTRACT

Kaya K., Optical Monitoring of Cerebral Blood Flow and Metabolism During Carotid Endarterectomy, Hacettepe University Graduate School of Health Sciences Doctor of Philosophy Dissertation in Program of Physiology, Ankara, 2022. Carotid endarterectomy (CEA) is a surgical operation to eliminate plaque in the carotid bifurcation where patients are at risk of embolic stroke. CEA requires cross-clamping of carotid arteries (common, internal, and external) to halt the blood flow in the surgical area, causing a hemodynamic challenge to the surgical hemisphere and the risk of embolus. Therefore, cerebral hemodynamics or electrophysiology is intraoperatively monitored via different modalities, including near-infrared spectroscopy (NIRS), electroencephalogram (EEG), somatosensory evoked potentials, carotid stump pressure, and transcranial Doppler ultrasound. Although EEG is a commonly used and reliable monitoring technique for CEA, it is a surrogate measure of cerebral blood flow (CBF). Further, different anesthetic regimens could suppress its waveforms, making it difficult to rely on to ensure adequate CBF. Furthermore, there has been no gold standard for monitoring CBF during CEA. Therefore, we aimed to investigate changes in CBF index (CBF_i) and cerebral metabolism via combined diffuse correlation spectroscopy (DCS) and NIRS system in patients who underwent CEA. We compared changes in EEG power spectra with cerebral hemodynamics on twenty-three CEA patients by quantifying a well-known EEG spectral method, desynchronization function. We also assessed different induction anesthesia on desynchronization functions to indicate electrophysiological and neurovascular changes with respect to clamping. Finally, we evaluated variability within CBF_i and EEG power spectra by quantifying the coefficient of variation to capture hemispheric differences. A combined DCS-NIRS system can deliver complementary cerebral hemodynamic assessment to electrophysiology during CEA. Furthermore, intraoperative monitoring of clamp-induced cerebral hypoperfusion with a combined DCS-NIRS system would help make acute management changes in inpatient care (e.g., arterial shunting). Assessing the electrophysiological and neurovascular status of the brain can avert undesirable events such as hypoperfusion and hypoxia, prevent cerebral ischemia and allow determining personalized perfusion strategies.

Keywords: Intraoperative neuromonitoring, carotid endarterectomy, diffuse correlation spectroscopy, cerebral blood flow, near-infrared spectroscopy, anesthesia

TABLE OF CONTENTS

ABBREVIATIONS

$\Delta r^2(\tau)$	Mean-squared Displacements of Scattering Particles
β	Coherence Parameter
θ	The Angle of Scatter
q	Momentum Transfer
ε	Extinction Coefficient
τ	Delay Time
$g_1(\tau)$	Normalized Electric Field Temporal Autocorrelation Function
$g_2(\tau)$	Normalized Temporal Autocorrelation Function
I_0	Light Intensity Changes
$K(\tau)$	Decay Rate at time τ
L	Distance Between Source and Detector
λ	Wavelengths
Δ_c	Changes in Absorber Concentration
Δ**I**	Changes in Light Intensity
Δ**OD**	Changes in Optical Density
$\Delta\mu_a$	Changes in Absorption Coefficient
μ_a	Absorption Coefficient
μ_s'	Reduced Scattering Coefficient
t	Time
[HbO]	Oxyhemoglobin Concentration
[HbR]	Deoxyhemoglobin Concentration
[HbT]	Total Hemoglobin Concentration
Δ**[HbO]**	Changes in Oxyhemoglobin Concentration

Δ[HbR]	Changes in Deoxyhemoglobin Concentration
Δ[HbT]	Changes in Total Hemoglobin Concentration
ABP	Arterial Blood Pressure
APD	Avalanche Photodiode Detector
BF_i	Blood Flow Index
CBF	Cerebral Blood Flow
CBF_i	Cerebral Blood Flow Index
CCA	Common Carotid Artery
CEA	Carotid Endarterectomy
CoW	Circle of Willis
CSP	Carotid Stump Pressure
$CV^{side}_{response}$	Coefficient of Variation of a Side and a Response
CW	Continuous-wave
***D*-index**	Minimum Value of Desynchronization Function
***D*(t)**	Desynchronization Function at time *t*
DCS	Diffuse Correlation Spectroscopy
DPF	Differential Pathlength Factor
ECA	External Carotid Artery
EEG	Electroencephalogram
FD	Frequency-domain
ICA	Internal Carotid Artery
IQR	Interquartile Range
KEA	Karotis Endarterektomi
MAC	Minimum Alveolar Concentration
MAP	Mean Arterial Pressure

MBLL	Modified Beer-Lambert Law
NIR	Near-infrared
NIRS	Near-infrared Spectroscopy
***P*(t)**	Power Changes at time *t*
$\boldsymbol{P_{ref}}$	Power of Reference Period
PSD	Power Spectral Density
RBC	Red Blood Cell
S	Slope
SD	Standard Deviation
SEM	Standard Error of The Mean
SKA	Serebral Kan Akımı
$\mathbf{SKA_i}$	Serebral Kan Akımı İndeksi
SNR	Signal-to-noise Ratio
$\mathbf{SO_2}$	Oxygen Saturation
SSEP	Somatosensory Evoked Potential
TCD	Transcranial Doppler
TD	Time Domain

LIST OF FIGURES

LIST OF TABLES

1. INTRODUCTION

"Natura valde simplex est et sibi consona."

Sir Isaac Newton

Carotid endarterectomy (CEA) is a surgery to remove atherosclerotic plaque at the carotid bifurcation. The mainstay of CEA surgery is to reduce the risk of embolic stroke by removing the plaque, which is mainly located in the vicinity of the internal carotid artery (ICA) and common carotid artery (CCA). CEA procedure entails cross-clamping of the three branches of the carotid artery (common, internal, and external) at the surgery side, leading to a complete cessation of blood flow (1). During the cross-clamping, stable cerebral blood flow (CBF) is ensured by cerebral autoregulation, whereby the ipsilateral brain hemisphere maintains oxygen-rich blood through the circle of Willis (CoW) and collateral circulation (2,3). Nevertheless, there may not be adequate delivery and compensation due to abnormal CoW anatomy and/or autoregulatory disturbance of cerebral hemodynamics. Therefore, cerebral electrophysiology and hemodynamics must be concomitantly assessed by different neuroimaging techniques during CEA.

Currently, electroencephalography (EEG) is the most feasible and commonly used intraoperative neuroimaging technique, among other eligible neuroimaging techniques (4,5). EEG is a noninvasive method of recording postsynaptic neuronal activity using either scalp or needle electrodes placed onto the skin. As a surrogate measure of CBF, EEG relies on deterioration in neuronal activity caused by prompt reduction in CBF and metabolism. However, different anesthetic regimens produce different changes in CBF and spectral EEG due to flow-metabolism coupling or decoupling, such as propofol with higher concentrations of sevoflurane (6,7). During CEA, EEG is examined in real-time through visual inspection from both raw and processed data (e.g., compressed spectral function) to detect cerebral hypoperfusion. While it is easy to interpret processed data than raw data, processed EEG may not contain substantial information due to conversion, leading to misinterpretation of EEG data (8,9). As a shunt is utilized with respect to changes in EEG data, this misinterpretation may trigger unnecessary use of a shunt and induce an embolic event.

Although EEG allows for identifying CBF variations in clinical practice as a surrogate measure, there are common limitations to EEG recordings during CEA. One requires the use of a specific anesthetic regimen that can allow reliable recordings since various anesthetic agents and their doses could suppress EEG waveforms. Thus, it can be difficult and challenging to rely on EEG to ensure adequate CBF (10). Another is dependent on expert clinical neurophysiologists who can interpret CBF adequacy or lack thereof upon clamping from the raw and/or processed EEG (5,11). These issues can be overcome by employing a complementary neuroimaging technique that could provide important insight into cerebral hemodynamics and improve the efficacy of detecting cerebral hypoperfusion and hypoxia.

Optical neuroimaging techniques have made notable progress in offering continuous, easy-to-use, and noninvasive cerebral hemodynamic monitoring devices for research and clinical practice (12–15). Near-infrared spectroscopy (NIRS) uses light attenuation on the well-known spectral window of the near-infrared (NIR) range (650 – 850 nm) wherein absorption of biological tissue enables quantifying concentrations of oxyhemoglobin ([HbO]), deoxyhemoglobin ([HbR]), total hemoglobin ([HbT]), and hemoglobin oxygenation (SO_2) (16,17). NIRS offers practicality over EEG as it does not require a gel or a paste to assure connectivity. While NIRS has a better spatial resolution to consider hemodynamic responses, EEG offers a better temporal resolution. Nevertheless, NIRS and EEG are complementary neuroimaging techniques that can be used simultaneously without cross-talk (18,19).

Diffuse correlation spectroscopy (DCS) is an emerging optical technique for noninvasively measuring a blood flow index (BF_i, cm^2/s) in biological tissues. Studies have shown that DCS can monitor BF_i in adults and neonates (12,13,20,21). DCS quantifies the temporal fluctuations in the intensity of the speckle pattern formed when coherent near-infrared light passes through biological tissue. This speckle pattern fluctuates by the drift of moving scatterers (e.g., erythrocytes) (22). The time of these fluctuations is then quantified by the normalized temporal autocorrelation function (g_2) from the detected light. By fitting the correlation diffusion equation to the g_2, DCS can quantify a BF_i in the illuminated tissue (23–26). The measuring perfusion index

provided by DCS can potentially offer critical information to the clinical team for preventing intraoperative complications of CEA (12,27).

As clamping causes a reduction in CBF and a decrease in relative alpha-band power with respect to the pre-clamping baseline, it can be a reliable indicator of cerebral ischemia (28). This approach has been demonstrated by the EEG desynchronization function (D(t)) in the 8–15 Hz band power reduction for patients who underwent CEA surgery (4). However, the real-time changes in neuronal and neurovascular responses and their interactions with anesthesia have not yet been elucidated. In this dissertation study, therefore, we used a combined DCS-NIRS system to monitor changes in CBF and hemoglobin concentrations about neuronal changes for patients who underwent CEA. The purpose of this dissertation is threefold:

Firstly, we aimed to show the feasibility of using a combined DCS-NIRS system to noninvasively and continuously acquire cerebral BF_i (CBF_i) and hemoglobin concentrations in conjunction with EEG recordings during CEA. Together, these measurements can provide important insight into electrophysiological and hemodynamic status of cerebral physiology to better indicate hypoperfusion and help to facilitate strategies for amplifying optimal cerebral perfusion during CEA.

Secondly, we hypothesized that the effect of clamping might be more notable in CBF_i data than in EEG power spectra. To address this hypothesis, we first calculated the EEG D(t), a slope of D(t), the minimum value (D-index), and the time-to-minimum of D(t) after clamping. Then, we applied the same methodology to the CBF_i data to obtain derivatives of D(t) to compare them with that of EEG in all patients. We also performed group comparisons between CBF_i and EEG power spectra according to the offline EEG classification (4,28).

Lastly, we hypothesized that the different anesthetics might induce different hemispheric neuronal and hemodynamic responses. To address this hypothesis, coupling between neuronal and neurovascular responses was examined for all induction anesthesia agents. We then quantified the coefficient of variation (CV) for each hemisphere to capture clamp-induced changes within 30–min for CBF_i and EEG.

2. BACKGROUND

2.1. Carotid Endarterectomy

The carotid bifurcation is an anatomical region where the CCA divides into the ICA and external carotid artery (ECA). While ICA provides blood flow to cerebral tissue, ECA provides blood flow to extracerebral compartments such as the skin and scalp. Carotid bifurcation has physiological importance as it contains baroreceptors and chemoreceptors that regulate homeostasis in response to acute changes in arterial blood pressure (ABP) and arterial oxygenation, respectively. Moreover, arterial vascularization of the head and neck area derives from the carotid and vertebral arteries, which make carotid bifurcation even more critical in different physiological and pathological processes (29).

The main arterial inflow is delivered to the brain via four major arteries: two ICAs and two vertebral arteries (Figure 2.1A). Eighty-to-ninety percent of the cerebral blood supply is delivered via the two ICAs, and the rest comes from the vertebrobasilar system (30). Therefore, ICAs are quantitatively the most important (31). The CoW ensures equal pressure on both hemispheres and does not allow crossing over the blood flow in normal conditions (Figure 2.1A, highlighted area). Moreover, the CoW offers considerable protection to the brain against occlusion. The CoW is located below the hypothalamus and is formed by the union of the carotid and vertebrobasilar arteries. The CoW is the origin of the six large vessels that supply blood flow to the almost entire cerebral cortex (Figure 2.1B).

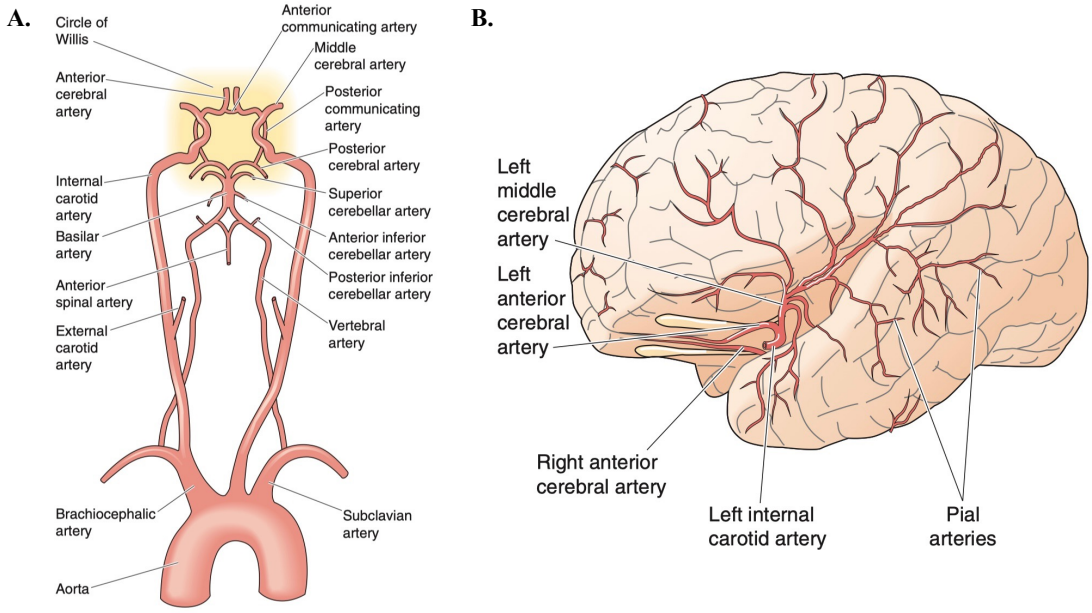

Figure 2.1. Illustration of the establishment of Circle of Willis (A, highlighted area) and vascular anatomy of the brain (B). The temporal lobe was pulled down in the B, exposing the left cerebral arteries and ICA. Pial arteries travel through the brain's surface and constitute penetrating arterioles to supply the microcirculation. The figure was taken and modified from (30).

Atherosclerosis mainly occurs at the carotid bifurcation (Figure 2.2A) that of 15–20% between CCA and ICA, especially in the region of the carotid sinus (Figure 2.2B). This built-up plaque can cause ischemic stroke through an embolus in the cerebral circulation that usually ends up in the anterior or posterior cerebral arteries. To provide normal CBF, as in Figure 2.2C, CEA is performed to eliminate this built-up plaque at the carotid bifurcation that requires clamping of three branches of the carotid artery (Figure 2.2D). During cross-clamping, ipsilateral CBF depends upon perfusion through collateral circulation and might be affected by changes in the collateral circulation, which is primarily dependent on contralateral circulation (1,32) (Figure 2.2E). Nonetheless, most strokes are due to embolization or thrombosis in nature, even though cross-clamping is a major hemodynamic challenge to the cerebral circulation.

Moreover, cerebral hypoperfusion and hypoxia might be triggered by inadequate collateral flow and impaired cerebral autoregulation (33). In addition, ischemic stroke can be induced by dissection, shunt utilization, and unclamping of the

carotid arteries. This hemodynamically impaired perfusion may also not be beneficial for CEA patients.

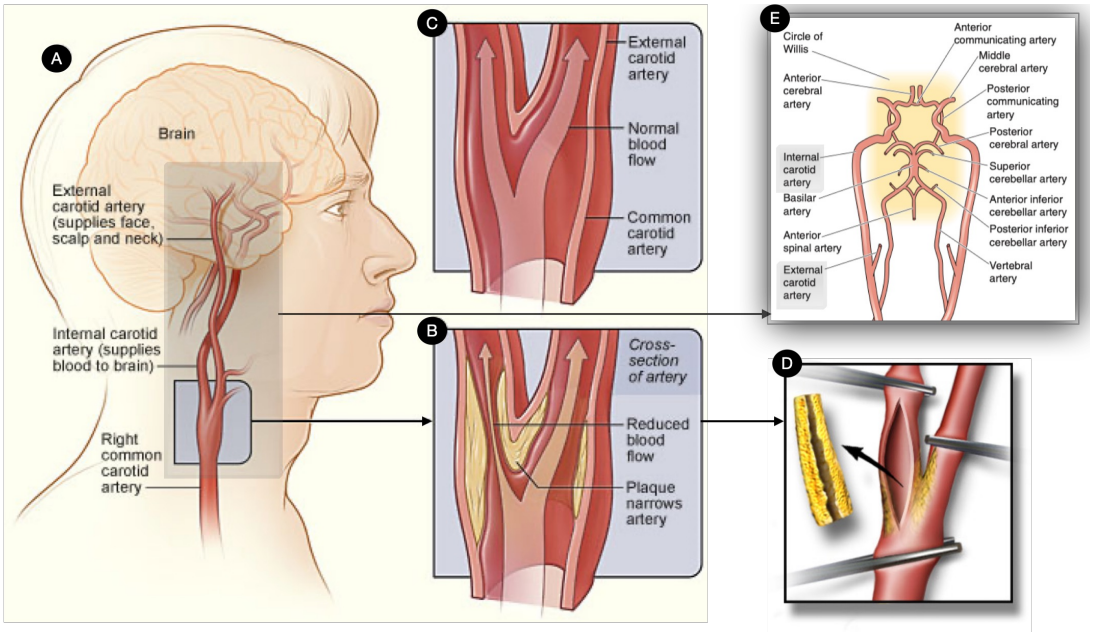

Figure 2.2. Illustration of the carotid bifurcation position on the neck (A). The CEA is performed to remove built-up plaque at carotid bifurcation (B) to restore normal blood flow (C). During the cross-clamping (D), CBF and metabolism are received from collateral circulation via CoW (E). Figure A, B, and C were taken from (34), D from (35), and E from (30).

2.1.1. Management of Cerebral Ischemia during CEA

To prevent cerebral ischemia, a shunt can be utilized as a primary intervention to provide supplemental blood flow from the CCA to the ICA upon cross-clamping (36). Additionally, systemic blood pressure can be increased at more than 20% of the preoperative level to maintain adequate CBF via the shunt, and thus, cerebral perfusion pressure can be maintained.

Although a carotid shunt may be beneficial since it provides supplemental CBF in patients with high-degree contralateral stenosis or abnormal CoW anatomy, it may trigger acute complications such as air or plaque embolization and intimal injury as well as other complications such as infection, nerve injury, hematoma, and carotid re-stenosis. Therefore, cerebral physiology should be intraoperatively monitored via

different neuromonitoring techniques to detect neurological and/or hemodynamic changes that may necessitate shunt utilization.

2.1.2. Intraoperative Neuromonitoring during CEA

CEA patients are often monitored intraoperatively via EEG, somatosensory evoked potential (SSEP), carotid stump pressure (CSP), transcranial Doppler (TCD) ultrasound, and NIRS (4,5,37). However, none of them is perfect in terms of ease of use, continuity of monitoring, signal source, and requirement of skilled personnel.

Both EEG and SSEP are noninvasive methods to measure postsynaptic neuronal activity. As surrogate measures of CBF, they can be effective in detecting cerebral ischemia and indicating abnormal CBF changes. However, they suffer from common limitations. First, anesthetic agents and their doses affect neuronal activities and could suppress EEG and SSEP waveforms, making them difficult to rely on to ensure adequate CBF (10). Second, the utility of these neurophysiologic tests depends on the availability of expert clinical neurophysiologists—finally, the requirement of using specific anesthetic regimens to allow reliable electrophysiological recordings. In addition, they are measurement-specific limitations for EEG and SSEP.

There are two types of EEG interpretation during CEA: raw and processed EEG. The interpretation of the real-time raw EEG is difficult because of requiring substantial skill and experience. Conversely, it is easier to interpret the real-time processed EEG. However, there is a significant loss of information during the conversion from raw to processed EEG (8,9). Furthermore, some patients' postoperative course results in neurological deficits even though no significant EEG/SSEP changes were shown during the CEA procedure (5,11).

SSEP offers some advantages over EEG in terms of detecting cerebral ischemia. In SSEP, information travels through a stimulated peripheral nerve carried by first- and second-order neurons and denotes an evoked response in the somatosensory cortex. Therefore, SSEP also examines the subcortical structures along with the cerebral cortex. Nevertheless, SSEP has remained as a theoretical approach and failed to indicate any particular advantage over EEG (38,39).

As distinct from SSEP and EEG, CSP and TCD ultrasound are perfusion-related measurements. CSP is measured at the distal end of the ICA after CCA and ECA are clamped. While indicating the collateral circulation efficiency of the CoW, CSP is a noncontinuous, invasive measurement, and the available evidence has failed to validate its efficacy (40). Several studies have shown that the sensitivity of CSP is not delicate to identify CEA patients who posed EEG changes with respect to cerebral ischemia upon cross-clamping (41,42). Furthermore, the pressure threshold of CSP established under general anesthesia is not well defined. Therefore, CSP is not a completely reliable neuromonitoring method for indicating neurological changes and cerebral hypoperfusion.

TCD ultrasound can measure blood flow velocity reductions in the middle cerebral artery to detect emboli and directly quantify the amount of cerebral hypoperfusion and its severity on neuronal function (43). However, TCD ultrasound is not generally adopted for intraoperative CEA monitoring because of the difficulty maintaining alignment with the middle cerebral artery for long periods, the inability to measure the proximal part of the cerebral arteries, and the need for a skilled technician (44). In addition, TCD ultrasound cannot be used on 10–15% of patients as they lack a sufficient temporal bone window (45).

2.1.3. Hemodynamic Changes during CEA

The compelling issue is the management of hypotension and hypertension episodes during the intraoperative course for hypertensive patients. Since hypertension is marked among CEA patients, cardiovascular perturbations are common in these patients under anesthesia (46,47). Consequently, ABP is markedly increased upon cross-clamping to avoid hypoperfusion. In the same manner, ABP is decreased upon unclamping to avoid hyperperfusion. The anesthetics and anesthetic regimen are also essential to maintain adequate cerebral perfusion since anesthetic agents affect cerebral hemodynamics differently. Sevoflurane facilitates less vasodilation than isoflurane at the same depth of anesthesia, although both provide rapid recovery (48).

Nevertheless, there are no precise data in favor of any anesthetic regimen with respect to CBF and metabolism. Studies have shown that some sevoflurane concentrations (i.e., 1.0 MAC) cause concomitant regional CBF reduction and metabolism in almost all areas (6), whereas some sevoflurane concentrations (i.e., 1.5 MAC) increase regional CBF in some regions (e.g., frontal cortex, thalamus, cerebellum) (49). In addition, anesthesia is usually maintained by propofol which leads to marked reductions in CBF and metabolism (50). Notably, different anesthetic agents yield marked CBF and metabolic rate reductions due to tight coupling. This is in contrast to the flow-metabolism decoupling in some anesthetic combinations, such as propofol with higher sevoflurane concentrations (6).

The postoperative course of CEA is notable for hypotension in 8–10% of patients and hypertension in 25–58% of patients (51). Indeed, postoperative deterioration in the sensitivity of the carotid baroreceptor reflex might cause postoperative hypotension or hypertension (52–54). This is probably due to transient mechanical injury in baroreflex sensitivity triggered by surgery (55).

2.2. Optical Brain Imaging

In recent years, optical neuromonitoring techniques have augmented our understanding of the hemodynamic origins of the brain by providing easy-to-use and bedside neuromonitoring devices (12,13). When NIR passes through to biological tissue via placed LEDs or optical fibers connected to lasers, optical changes of illuminated tissue (e.g., absorption or scattering) can be quantified by an optical detector placed at a distance from the source. By quantifying these properties, we can noninvasively monitor changes in CBF and metabolism. Although there are several ways of employing NIR diffuse optical spectroscopies, we will primarily focus on continuous-wave NIRS (CW-NIRS) and DCS in this dissertation study.

2.2.1. Near-infrared Spectroscopy

NIRS is a noninvasive neuroimaging technique that quantifies light attenuation by emitting multiple wavelengths in the optical spectrum of 650 – 850 nm to quantify

regional concentration changes in [HbO], [HbR], and [HbT] (Δ[HbO], Δ[HbR], and Δ[HbT], respectively) of the mixed arterial, capillary, and venous bed under the optical probe placed onto the skin (16). There are three types of NIRS modalities: 1) CW-NIRS, 2) frequency-domain NIRS (FD-NIRS), and 3) time-domain NIRS (TD-NIRS). Absolute optical properties can be measured by FD-NIRS or TD-NIRS systems, which utilize light pulses or sinusoidally modulated light. These modalities also allow quantifying absolute [HbO] and [HbR] (56). This is in contrast to CW-NIRS (a.k.a. functional NIRS), which quantifies relative concentration changes with respect to a baseline. By employing the optical tissue properties in the literature (57), the amount of hemoglobin oxygenation can be calculated by CW-NIRS. Using the modified Beer-Lambert law (MBLL), we can quantify Δ[HbO], Δ[HbR], and Δ[HbT]. The benefit of MBLL is to characterize the relationship between light intensity and light absorption in the illuminated tissue.

To measure changes in hemoglobin concentrations, absorption coefficient changes of light ($\Delta\mu_a(\lambda)$) from at least two wavelengths (λ) must be measured. MBLL (Eq. 1) denotes the light intensity changes ($\Delta I(\lambda)$) relative to the baseline light intensity changes ($I_0(\lambda)$). This can be translated into $\Delta\mu_a(\lambda)$ at a distance (L) between the source and detector (58):

$$\Delta\mu_a(\lambda) = \frac{-1}{DPF \cdot L}\frac{\Delta I(\lambda)}{I_0(\lambda)} \qquad \text{Eq. 1}$$

$$DPF = \frac{\sqrt{3\mu_s'(\lambda)}}{2\sqrt{\mu_a(\lambda)}} \qquad \text{Eq. 2}$$

The differential pathlength factor (DPF, see Eq. 2) is a function in which absorption coefficient (μ_a) and reduced scattering coefficient (μ_s') are used to assume the absolute optical properties of tissue. DPF delineates the average distance that light travels through the biological tissue, which is approximately equal to 6 for human measurements. DPF can be assumed from literature for CW measures or obtained by

FD or TD systems. Δ[HbO] and Δ[HbR] can be derived by assuming the molecular light extinction coefficient (ε) of HbO and HbR from literature (59):

$$\Delta\mu_a(\lambda) = \sum_n \varepsilon_n(\lambda) \cdot \Delta c_n \qquad \text{Eq. 3}$$

where Δc_n is the concentration changes of all absorbers. Using at least two λ, we can distinguish two absorbers (i.e., HbO and HbR). As other absorbers are primarily constant during a measurement, we can assume constants for other absorbers from literature, including water, lipids, and melanin.

2.2.2. Diffuse Correlation Spectroscopy

DCS is an emerging optical technique that can directly and noninvasively measure a BF_i. Briefly, DCS quantifies speckle interference patterns formed by coherent NIR. The speckle pattern fluctuates by moving scatterers (e.g., erythrocytes) (22). The time of these fluctuations is quantified by the $g_2(\tau)$ from the detected light (see Eq. 4).

$$g_2(\tau) = \langle I(t)I(t+\tau)\rangle / \langle I(t)\rangle^2 \qquad \text{Eq. 4}$$

By fitting the correlation diffusion equation to the $g_2(\tau)$ curve, DCS can quantify a BF_i in different compartments depending on the decay rate as illustrated in Figure 2.3 (23,24,26). The details about the quantification of BF_i are as follows.

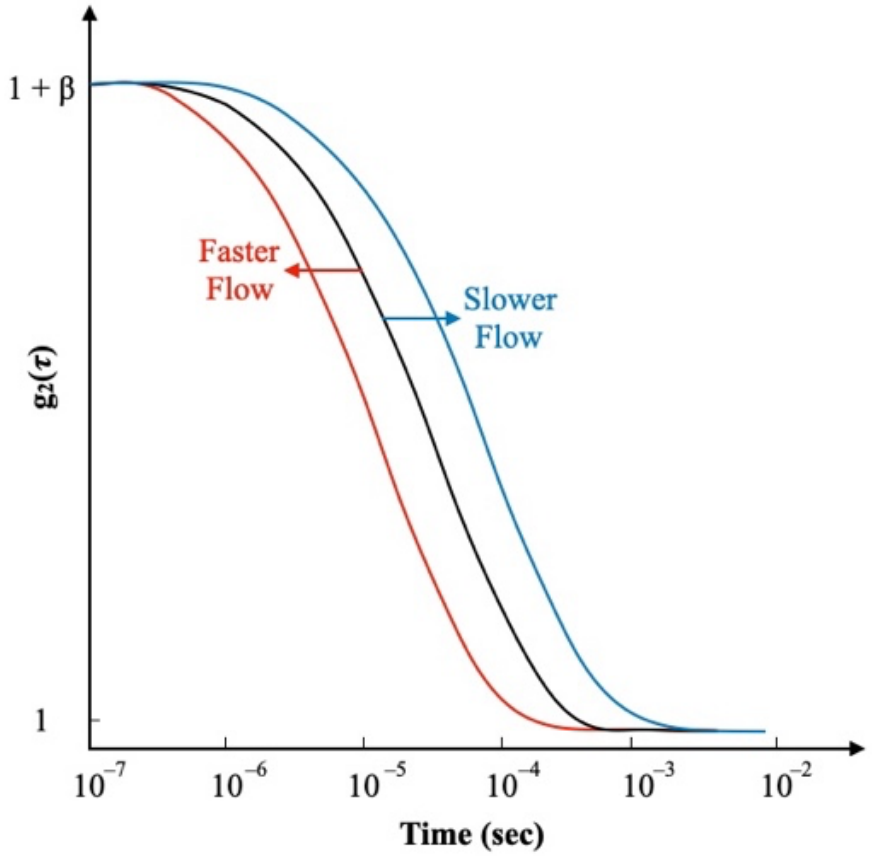

Figure 2.3. Illustration of normalized intensity autocorrelation function decay. Faster decay indicates faster blood flow (e.g., brain), while slower decay indicates slower flow (e.g., skin/scalp).

When a beam of coherent laser light travels through a turbid medium, the light is scattered and emerges from the media as an intensity pattern that composes many bright and dark spots called speckles. Since the scattering particles in the turbid medium are moving, the speckle pattern and the light intensity fluctuate over time. This time-varying intensity is detected by an avalanche photodiode detector (APD). For the single scattering case, the angle of scatter, θ, and the particle's motion determines the decay rate of the correlation function. Therefore, blood flow in tissue can be estimated by quantifying the time scale of the fluctuations using the electric field temporal autocorrelation function ($g_1(\tau)$, Figure 2.4A). More specifically, quantifying the decay of the correlation function provides information about the mean-squared displacements of scattering particles, $\langle \Delta r^2(\tau) \rangle$, in tissues such as red blood cells (RBCs), which are approximated quite well as an effective Brownian motion

(21,24,60,61). Therefore, we can obtain quantitative information on particle motions by measuring the temporal fluctuations of scattered light (62).

Expanding to the multiple scattering case, which is more realistic when modeling DCS measurements, light is scattered numerous times by RBCs in tissue. Photons reaching the detector typically follow different trajectories through the medium (Figure 2.4B). Under these conditions, the correlation function can be calculated within the same framework as a single-scattering event. In addition, since the photon diffusion model in DCS depends on the optical properties of tissue (i.e., μ_a and μ_s'), they are either assumed from the literature or measured by more advanced systems (e.g., FD or TD) (63,64).

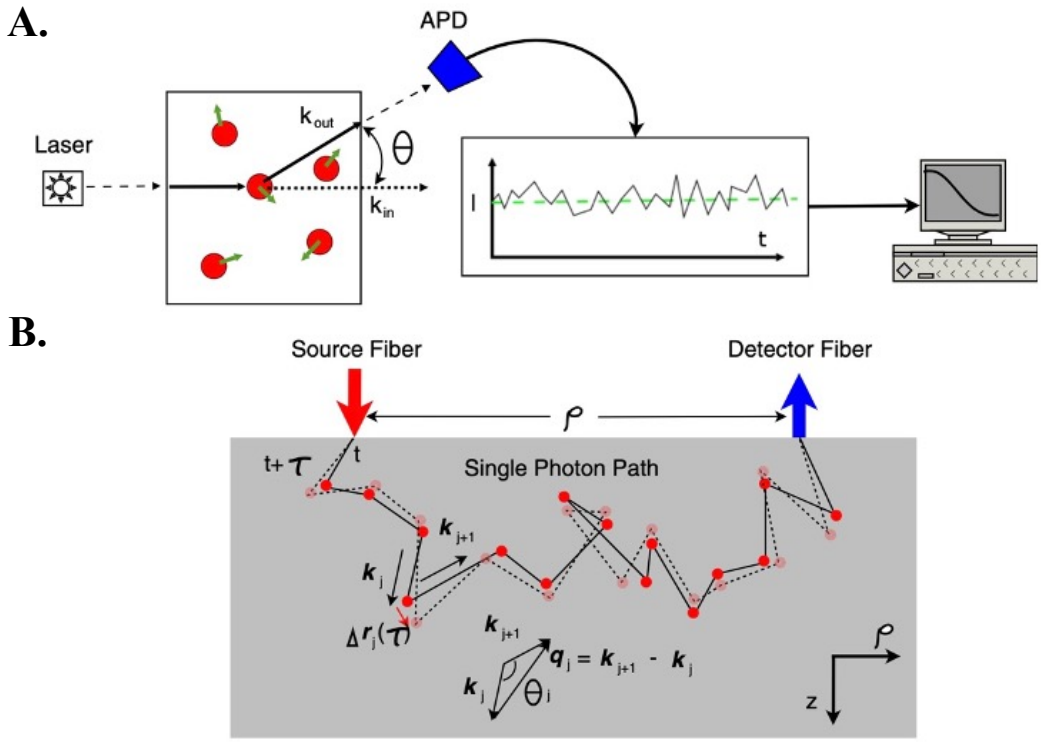

Figure 2.4. Illustration of a single scattering event (A) and multiple scattering events (B) along a single photon path in turbid media. k is the wavevectors for each event (j^{th}). q is the momentum transfer, and θ is the scattering angle of each scattering. The solid line represents the photon path at time t, while the dotted line represents the photon path at time t + τ. During the delay time τ, the scatterer moves $\Delta r_j(\tau)$. The figure was taken and modified from (22).

Because optical detectors measure light intensity instead of the electric field, a model connecting the $g_1(\tau)$ to $g_2(\tau)$ is required. The Siegert relation (see Eq. 5) is then used to extract the electric field autocorrelation function from the intensity data (65). Since the decay rate ($K(\tau)$) is determined by fitting $g_1(\tau)$ (see Eq. 6), this information and optical tissue properties allow for the extraction of the tissue BF_i (see Eq. 7).

$$g_2(\tau) = 1 + \beta|g_1(\tau)|^2 \quad \text{Eq. 5}$$

$$g_1(\tau) = \frac{\exp(-K(\tau) * r_1}{r_1} - \frac{\exp(-K(\tau) * r_b}{r_b} \quad \text{Eq. 6}$$

$$K(\tau) = \sqrt{3\mu_a\mu_s' + 6k_0^2\mu_s'^2(BF_i\tau)} \quad \text{Eq. 7}$$

where β is known as the coherence parameter in Eq. 5, and for typical DCS experiments taken in the reflection geometry with a high coherence laser source, is equal to 0.5.

DCS has been validated by several studies towards 'gold standard' methods in humans (24,66), animals (67–69), and human neonates (70). Furthermore, DCS has an enormous potential to differentiate pathologic conditions (71–74), and DCS-derived indices, such as cerebral autoregulation and cerebrovascular resistance, hold promise for inpatient care (12,75,76).

3. MATERIALS and METHOD

3.1. Study Patients and Procedure

We enrolled twenty-six patients who underwent CEA between September 2016 and January 2021 at the Massachusetts General Hospital. After compliance of potential CEA patients with inclusion criteria, the study was introduced to the patients by a physician during their preoperative visit. After providing sufficient time to evaluate whether to participate, CEA patients signed the informed consent. This study was reviewed and approved by the Massachusetts General Hospital and Mass General Brigham Institutional Research Board (#2015P002669). This study was supported by the National Institutes of Health grants R01GM116177 and R01HD0091067.

Twenty-three patients (age 69 ± 8, range 53-90, 10 females) were included in this study. One patient was excluded due to a lack of EEG data, one was excluded due to a hardware issue, and one was excluded because the optical probe was placed on the temporal rather than a prefrontal area for evaluation of the signal quality at the very beginning of the study. Table 3.1 indicates the remaining patients' demographics, optical measurements, duration of measurement and clamping, degree of ipsilateral and contralateral stenosis, and comorbid diseases.

Table 3.1. Measurement and patients' clinical characteristics.

Patient	Age	Weight (kg)	Height (cm)	Sex	Optical Measurement	Measurement Duration	Clamp Duration	Degree of Stenosis	
								Ipsilateral	Contralateral
1	70	70	168	F	Unilateral	2 h, 52 min	48 min	70–89%	No stenosis
2	62	98	178	M	Unilateral	2 h, 29 min	53 min	70–89%	1–19%
3	73	73	157	F	Unilateral	2 h, 20 min	1 h, 4 min	20–49%	No stenosis
4	64	89	175	F	Unilateral	3 h, 58 min	1 h, 19 min	70–89%	20–49%
5	66	87	175	M	Unilateral	2 h, 19 min	1h, 1 min	90–99%	1–19%
6	70	113	175	M	Unilateral	3 h, 53 min	40 min	1–19%	1–19%
7	77	89	177	M	Unilateral	3 h, 17 min	1 h, 17min	20–49%	1–19%
8	74	113	173	M	Bilateral	3 h, 34 min	58 min	70–89%	70–99%
9	53	49	160	F	Bilateral	3 h, 14 min	52 min	70–89%	No stenosis
10	64	160	74	F	Bilateral	2 h, 48 min	55 min	70–89%	1–19%
11	68	95	175	M	Bilateral	2 h, 48 min	1 h, 5 min	70–89%	20–49%
12	90	86	172	M	Bilateral	2 h, 25 min	1 h, 3 min	70–89%	No stenosis
13	67	77	168	F	Bilateral	1 h, 35 min	37 min	70–89%	No stenosis
14	63	74	165	F	Bilateral	2 h, 27 min	1 h, 3 min	20–49%	1–19%
15	78	77	173	F	Bilateral	2 h, 33 min	49 min	70–89%	1–19%
16	66	98	191	M	Bilateral	1 h, 53 min	46 min	50–69%	100%
17	56	78	183	M	Bilateral	2 h, 47 min	1 h, 1 min	70–89%	1–19%
18	69	107	183	M	Bilateral	2 h, 55 min	1 h, 4 min	70–89%	20–49%
19	74	85	163	F	Bilateral	2 h, 11 min	43 min	70–89%	50–69%
20	66	100	160	F	Bilateral	2 h, 24 min	56 min	50–69%	1–19%
21	80	77	170	M	Bilateral	4 h, 04 min	1 h, 34 min	70–89%	No stenosis
22	65	73	165	M	Bilateral	1 h, 15 min	53 min	70–89%	70–89%
23	64	90	168	M	Bilateral	2 h, 02 min	56 min	70–89%	50–69%

Age, year (mean ± SD)	69 ± 8
Range	53 – 90
F:M	10:13
Comorbid Disease	*n* = 23
Hypertension	78%
Diabetes-Mellitus	39%
Coronary Disease	26%
Hyperlipidemia	48%
Atrial Fibrillation	13%

During the surgery day, one or two optical probes (Figure 3.1A, indicating probe geometry) were secured to the patient's forehead alongside the clinically used EEG electrodes during preoperative procedures (Figure 3.1B). Measurements were taken in the operating room from general anesthesia induction until the end of anesthesia administration.

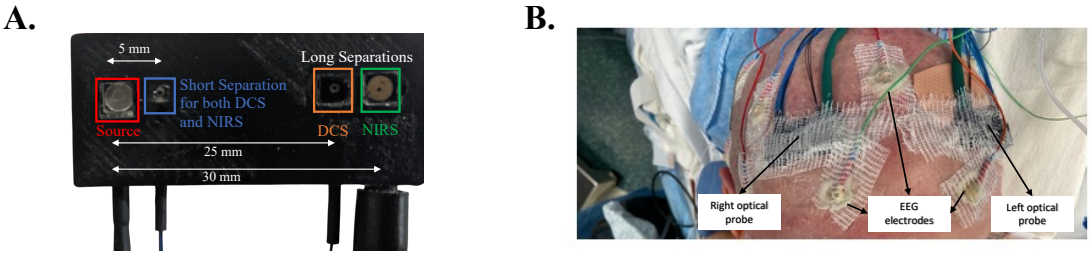

Figure 3.1. (A) The DCS-NIRS probe. Red square is the co-localized DCS and NIRS source fiber, blue is the co-localized DCS and NIRS short separation detector fiber, orange is the DCS long separation detector, and green is the NIRS long separation detector. (B) The optical probes after bilateral placement on patient #21. The figure was taken and modified from (12).

Anesthesia induction was carried out intravenously via propofol with sevoflurane, propofol with isoflurane, and propofol alone. Anesthesia was also maintained with a bolus of propofol. In some patients, fentanyl or remifentanil, and an additional NO_2 mixture were also used for anesthesia maintenance. An expert neurophysiologist visually inspected raw and processed EEGs during the CEA procedure. Based on the intraoperative inspection, the shunt utilization was decided in three patients (#5, 11, and 20) due to immediate EEG changes and slowing down in fast frequencies after 1–2 min clamping. On one patient (#10), the shunt decision was planned preoperatively, as the patient may have encountered hemodynamic challenges given the patient's stroke history and cardiovascular diseases (Table 3.2). For muscle relaxation, some additional drug is also administered to facilitate tracheal intubation such as lidocaine.

Table 3.2. Anesthesia induction, maintenance, and shunt utilization.

Patient	Shunt	Induction			Maintenance		
		Propofol	Sevoflurane	Isoflurane	Fentanyl	Remifentanil	NO_2
1	No	100 mg		0.8%	100 γ	80 γ	75%
2	No	150 mg		0.8%	50 γ		
3	No	100 mg	1.0%		100 γ		
4	No	150 mg	1.5%		150 γ		
5	Yes	120 mg	1.0%		25 γ		50%
6	No	100 mg		0.6%	100 γ		55%
7	No	100 mg	1.0%		200 γ		50%
8	No	100 mg	1.0%		100 γ		
9	No	100 mg	1.0%		75 γ		50%
10	Yes	100 mg	1.5%		75 γ		
11	Yes	100 mg	0.8%		50 γ		70%
12	No	100 mg				150 γ	
13	No	100 mg	1.1%				
14	No	100 mg					
15	No	100 mg	0.6%				
16	No	100 mg				150 γ	
17	No	100 mg	2.0%		100 γ		
18	No	100 mg				150 γ	
19	No	150 mg			100 γ	150 γ	50%
20	Yes	200 mg		0.5%	100 γ	100 γ	
21	No	100 mg	1.0%		100 γ		50%
22	No	100 mg	0.7%		100 γ		50%
23	No	100 mg	1.0%		100 γ		50%

3.2. Optical Measurements and Clinical Auxiliary Signals

We acquired unilateral CBF_i in the first seven patients via DCS on the ipsilateral forehead to the surgery side. In the next three patients (#8, 9, and 10), we acquired bilateral CBF_i. In all other patients (13 patients), we employed bilateral DCS and NIRS measurements. Clinical physiological recordings were co-acquired during our measurements, including electrocardiogram, EEG, and ABP. The mean arterial pressure (MAP) was computed by

$$\mathrm{MAP} = \frac{\mathrm{Pressure}_{\mathrm{systolic}} + 2 \times \mathrm{Pressure}_{\mathrm{diastolic}}}{3} \quad \text{Eq. 8}$$

For optical measurements, we used the MetaOx system (ISS Inc. Champaign, IL), which has FD-NIRS and DCS components (64). The DCS component contains a long-coherence length laser at 850 nm and eight single-photon counting avalanche photodiode detectors. For all DCS measurements, we used short and long separations of 5 and 25 mm (except for patient #10, who had separations of 5 and 30 mm) for the superficial (extracerebral) and brain-sensitive measurements, respectively. DCS long separation detected lights from three detectors to improve the signal-to-noise ratio (SNR).

The NIRS component contains eight diode lasers emitting at different λ ranging from 670 to 830 nm and four photomultiplier tube detectors. For NIRS measurements, we used source-detector separations of 5 and 30 mm for short and long separations, respectively. The longer separation with NIRS (30 mm instead of 25 mm) was chosen to account for the lower penetration sensitivity of NIRS with respect to DCS (77). NIRS data were analyzed using MBLL under pathlength and initial hemoglobin concentration assumptions (16).

To achieve bilateral measurements, an external DCS system was added to systems with a long-coherence length laser at 850 nm (CrystaLaser). Eight diode lasers of NIRS were divided into two probes: the right forehead probe emitted λ of 672, 706, 759, and 830 nm, and the left forehead probe emitted λ of 690, 726, 784, and 813 nm.

3.3. Optical Data Processing

Optical data were analyzed using an in-house MATLAB (ver. R2018a, MathWorks Inc) pipeline. DCS intensity temporal autocorrelation function was acquired at 2 Hz for patients #1–10 and at 10 Hz for the remaining patients. DCS and MAP data were down-sampled to 0.2 Hz for 5–sec resolution via a windowed averaging of g_2 traces to enhance the SNR. To obtain a BF_i signal, the g_2 curves at each source-detector separation were fitted using the correlation diffusion equations for a semi-infinite medium (22) by assuming a fixed $\mu_a = 0.2$ cm^{-1} and $\mu_s' = 8.0$ cm^{-1} for all subjects (78). The signal was then smoothened by sliding window averaging (4 data samples = 20 sec) using the $smooth$ function built in MATLAB.

NIRS data from ten patients (patients #11–14, 17–21, and 23) were used for this analysis. Three patients were excluded due to hardware issues (patients #15, 16, and 22). The raw NIRS intensity data were also down-sampled to 0.2 Hz from 10 Hz via a windowed averaging. The changes in optical density (ΔOD) were converted into Δ[HbO], Δ[HbR], and Δ[HbT] using the MBLL (16). To fit the absorption coefficients at four λ per probe, we first calculated μ_a at each wavelength by using extinction coefficients (ε) in the literature (59) with an assumed 75% concentration of water (79). We also assumed an initial [HbO] of 50 μMol, [HbR] of 30 μMol, and [HbT] of 80 μMol. DPF was assumed at each wavelength following a scattering decay of $\mu_s' = 8.0 \times (\lambda/850)^{-1.5}$. Calculated μ_a, μ_s', and DPF values in each λ for the right and left forehead probes are indicated in Table 3.3.

Table 3.3. μ_a, μ_s', and DPF values of right and left forehead probe.

Forehead Probe	λ (nm)	μ_a (cm^{-1})	μ_s' (cm^{-1})	DPF
Right	672	0.26	11.38	5.78
	706	0.17	10.57	6.77
	759	0.21	9.48	5.84
	830	0.19	8.29	5.60
Left	690	0.20	10.94	6.41
	726	0.16	10.13	6.87
	784	0.18	9.03	6.19
	813	0.18	8.55	6.01

3.4. EEG Recordings and Data Analysis

EEGs were acquired using a Natus system (Middleton, WI) at a sampling frequency of 512 Hz (#21), 256 Hz (#1 and 2), and 250 Hz for the rest of the patients. Scalp electrodes were placed with respect to the 10–20 International System with linked-ear reference (A1 and A2) and ground in Fpz. Postsynaptic potentials were acquired via 19 Ag/AgCl scalp electrodes (Fp1, Fp2, Fz, F3, F4, F7, F8, Cz, C3, C4, T3, T4, T5, T6, Pz, P3, P4, O1, and O2). The impedance level was maintained at less than five kΩ for each channel.

During the preprocessing, electrodes of interest were defined as the left hemisphere (Fp1, F3, F7, C3, P3, T3, T5, and O1) and the right hemisphere (Fp2, F4, F8, C4, P4, T4, T6, and O2). Then, a Butterworth bandpass filter of 0.05 – 40 Hz was applied using a second-order zero phase shift to remove baseline drift and high-frequency noise. The EEG data were then detrended with polynomial order of twenty and tapered by 300–sec Hanning's window. Further, power spectral density (PSD) was estimated using the $pwelch$ function built into MATLAB. Averaged PSDs within the 8–15 Hz band were then extracted from a 1–min pre-clamping period to serve as a reference and a 5–min post-clamping period.

For the reference period, PSDs were estimated every 2–sec, and thirty single PSDs were averaged to obtain a single spectral index in each electrode. Post-clamping PSDs were calculated from the 20–sec sliding window or one epoch in each electrode, which allows for reliable spectral content. Each sliding window was shifted for 2–sec and partially overlapped with the previous epoch to allow a temporally reliable trend of the power spectrum (Figure 3.2). Finally, an averaged spectral index was obtained in each hemisphere by averaging the power spectra of each electrode of interest.

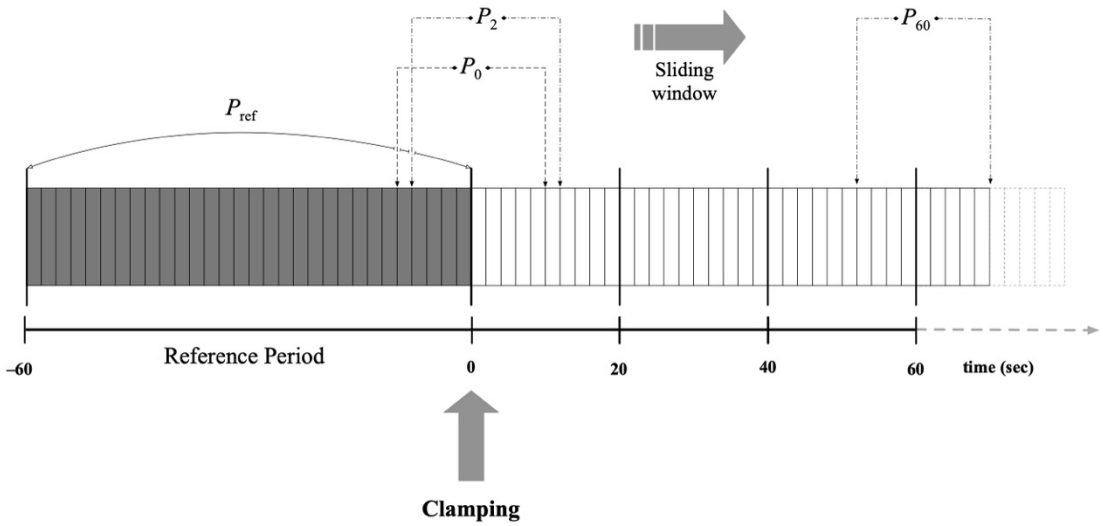

Figure 3.2. Schematic representation of desynchronization function analysis. Each rectangle denotes a 2–sec epoch. Reference power (P_{ref}) within 1–min pre-clamping time was obtained by means of averaging thirty epochs, indicated by dark rectangles. Clamp-induced power spectra changes (P) at time t are estimated via averaging the spectral power of each epoch (20–sec) with a 2–sec time shift. The figure was taken and modified from (4).

The desynchronization function D(t) was then allocated (Eq. 9) with respect to the averaged alpha band power of the pre-clamping or reference phase (P_{ref}) by

$$D(\mathrm{t}) = \frac{P(\mathrm{t}) - P_{\mathrm{ref}}}{P_{\mathrm{ref}}} \times 100 \qquad \text{Eq. 9}$$

where P(t) is the 8–15 Hz band power centered at time t. This function is designed to determine the percentage of power modification during clamping with respect to the P_{ref}.

After calculation of the D(t), the minimum value and the time of this value during the 1–min period of post-clamping were defined as D-index and time-to-minimum, respectively. Since most drastic changes in D(t) occur within 30–sec upon

clamping (t_0), the slope index (*S*) was calculated to quantify the rate of response within this period (Eq. 10) by

$$S = \frac{D(t_0 + 30) - D(t_0)}{30} \quad \text{Eq. 10}$$

3.5. Comparing Clamp-induced CBF_i and EEG Changes

Changes in CBF_i and EEG spectral power were compared by employing the same desynchronization method for CBF_i. To perform the same methodology, the relative CBF_i ($rCBF_i$) was obtained with respect to 1–min pre-clamping baseline ($\text{relative} = \frac{\text{response}}{\text{baseline}}$), followed by allocating derivatives of *D*(t), slope, *D*-index, and time-to-minimum responses.

During the post-processing, patients were divided into three groups with respect to changes in EEG power spectra (4,28).

- Group A: patients with major EEG changes (*D*-index ≥ 50%)
- Group B: patients with moderate EEG changes (25%> *D*-index <50%)
- Group C: patients with no EEG changes (*D*-index ≤ 25%)

CBF_i and EEG power spectra were assessed with respect to induction anesthesia as (1) propofol alone, (2) propofol with isoflurane, and (3) propofol with sevoflurane to evaluate coupling or decoupling between neuronal and neurovascular responses. Finally, the variability within CBF_i and EEG spectral power according to induction anesthesia was assessed by the coefficients of variation (CV) method. The CV is a ratio of standard deviation to the mean, which allows the comparison of the degree of variation between different time series. The CV of CBF_i and EEG spectral power data was computed by using a 20–sec sliding window with 2–sec overlap for ipsilateral and contralateral hemispheres ($CV^{ipsi}_{response}$ and $CV^{contra}_{response}$, respectively) within the period of 3–min pre-clamping to 30–min post-unclamping.

3.6. Statistical Analyses

All statistical analyses were carried out using IBM SPSS (ver. 26, IBM Corp). The independent sample *t*-test was performed to investigate differences in *D*-index, *S*, and time-to-minimum between CBF_i and EEG *D*(t) for all patients. The same analysis was also conducted to compare $CV_{response}^{ipsi}$ and $CV_{response}^{contra}$ for all patients. Statistical significance was assessed by using a two-tail *t*-distribution with a 95% confidence interval. To compare CBF_i and EEG *D*(t) with respect to three power spectra groups (e.g., A, B, and C), the Mann-Whitney U test was performed.

To assess the different anesthetic agents within CBF_i and EEG power spectra, a one-way analysis of variance (ANOVA) test was performed for *D*-index, *S*, time-to-minimum, $CV_{response}^{ipsi}$, and $CV_{response}^{contra}$, followed by a Tukey post hoc test for pairwise comparisons. To compare different responses (e.g., *D*(t) and CV) in the same anesthetics agents, the Mann-Whitney U test was performed to further elucidate the relation between CBF_i and EEG power spectra.

Data are represented as mean ± standard error of the mean (SEM) for parametric tests and median with interquartile range (IQR) as (median, IQR) for non-parametric tests unless otherwise noted. CV results are also represented as percentages. For all tests, *P*-value < 0.05 was considered statistically significant.

4. RESULTS

4.1. Hemodynamic Changes During Carotid Endarterectomy

The average duration of the surgery was 162 ± 44 min (standard deviation), and the average CEA time was 58 ± 13 min. Figure 4.1 indicates a typical measurement from a patient (#21). Carotid cross-clamping caused a marked decrease in ipsilateral CBF_i (Figure 4.1A). The reductions in ipsilateral CBF_i also caused a decrease of Δ[HbO] and an increase of Δ[HbR] (Figure 4.1B and C, respectively). Once ipsilateral CBF_i reached a minimum value, it was weakly recovered over a short period and congregated to a new value lower than the pre-clamping value during plaque removal (Figure 4.1A, after clamping). An increase of blood volume (Δ[HbO] + Δ[HbR]) was observed in the ipsilateral hemisphere during the clamping. This led to a slight recovery of CBF_i (Figure 4.1A–C, respectively).

Upon unclamping, there was a marked overshoot in CBF_i and Δ[HbO], and a decrease in Δ[HbR] on the ipsilateral side. After the overshoot, CBF_i and Δ[HbO] - Δ[HbR] recovered to the pre-clamping value, but at different rates. CBF_i recovered slowly (after 30 minutes), whereas Δ[HbO] and Δ[HbR] reached their pre-clamping value more rapidly (Figure 4.1A–C, respectively). The slow recovery in CBF_i was likely due to the medically reduced MAP to reduce the risk of bleeding and reperfusion injury with the post-clamping. MAP was also elevated during clamping (9 ± 12%), and reduced (11 ± 10%) starting pre-unclamping and continued post-unclamping (Figure 4.1D).

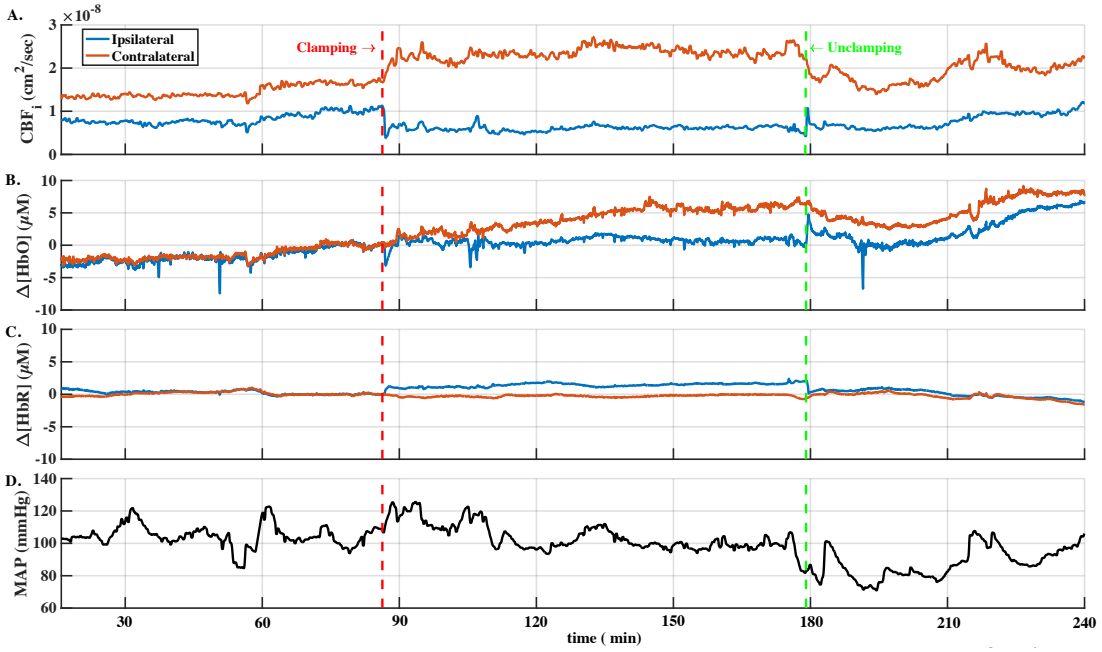

Figure 4.1. A typical CEA time course from a patient (#21). Ipsilateral and contralateral responses are demonstrated in blue and orange, respectively, for CBF_i (A), Δ[HbO] (B), and Δ[HbR] (C). MAP was invasively measured via an arterial cannula in the arm and is demonstrated in black (E). Clamping and unclamping are demonstrated as red and green dashed lines, respectively.

4.2. Quantification of Desynchronization Function

Figure 4.2 indicates a time course of *D*(t) of EEG and CBF_i from a patient (#21). The *D*-index of –68% was reached by CBF_i within 15 sec (Figure 4.2, bottom), whereas EEG reached its minimum value of –25% within 26 sec (Figure 4.2, top). While EEG *D*(t) also showed fluctuations over 2–min, CBF_i *D*(t) showed a constant recovery. Table 4.1 summarizes the *D*(t) results of CBF_i and EEG power spectra.

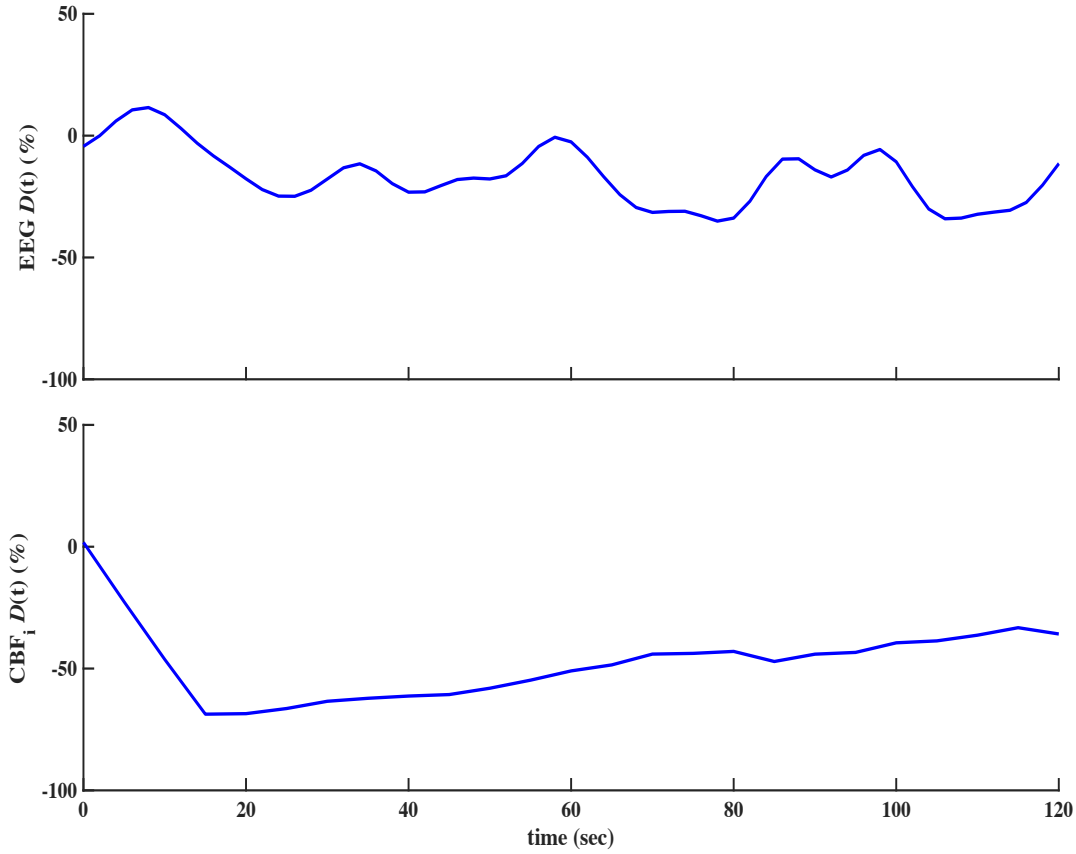

Figure 4.2. Desynchronization function, *D*(t), time course from a patient (#21). The time zero denotes clamping. The top panel indicates *D*(t) for EEG and the bottom panel indicates for CBF_i for the first 2–min of clamping.

Table 4.1. The results of *D*-index, slope, and time-to-minimum for CBF_i and EEG power spectra in each patient.

Patient	CBF_i			EEG		
	D-index (%)	Slope	Time-to-minimum (sec)	*D*-index (%)	Slope	Time-to-minimum (sec)
1	-57.57	-1.21	25	-5.74	-0.10	22
2	-76.50	-2.05	25	-10.64	-0.73	18
3	-50.04	-1.46	30	-33.17	-0.82	16
4	-55.88	-1.51	20	-43.78	-0.57	38
5	-45.93	-1.60	40	-30.30	-1.00	36
6	-69.00	-1.96	20	-14.96	0.19	20
7	-56.12	-1.68	20	-42.67	-1.04	16
8	-36.01	-0.07	15	-21.24	-0.35	32
9	-51.68	-1.21	25	-29.01	-1.52	56
10	-40.58	-1.34	35	-29.30	-1.62	18
11	-52.70	-1.70	20	-43.09	-2.19	60
12	-11.55	-0.72	60	-58.94	2.44	36
13	-49.80	-0.66	30	-33.74	-0.54	8
14	-26.23	-0.48	15	-62.89	-2.10	50
15	-70.90	-2.04	30	-25.88	0.54	18
16	-69.97	-2.14	35	-36.42	-0.01	22
17	-58.19	-2.08	20	-40.89	-1.08	14
18	-82.63	-3.01	35	-26.32	-0.70	54
19	-52.55	-1.74	55	-29.54	-0.11	38
20	-63.82	-1.72	20	-33.68	-0.28	14
21	-68.73	-1.76	15	-24.89	0.04	26
22	-54.65	-1.46	40	-99.97	-3.42	54
23	-57.91	-2.21	25	-42.92	-1.76	34

The *D*-index changes in EEG (36 ± 4%) was significantly lower than CBF_i (55 ± 3%, $t_{44} = 3.6$, $P = 0.001$, Figure 4.3 left). The slope changes in EEG ($S = 1 \pm 0.19$) was significantly lower than CBF_i ($S = 1.6 \pm 0.13$, $t_{44} = 3.1$, $P = 0.02$, Figure 4.3 middle), indicating faster decrease in CBF_i. Although time-to-minimum was attained faster in CBF_i (28 ± 2 sec) than EEG (30 ± 3 sec), there was no statistically significant differences for time-to-minimum ($t_{44} = 0.5$, $P = 0.64$, Figure 4.3 right).

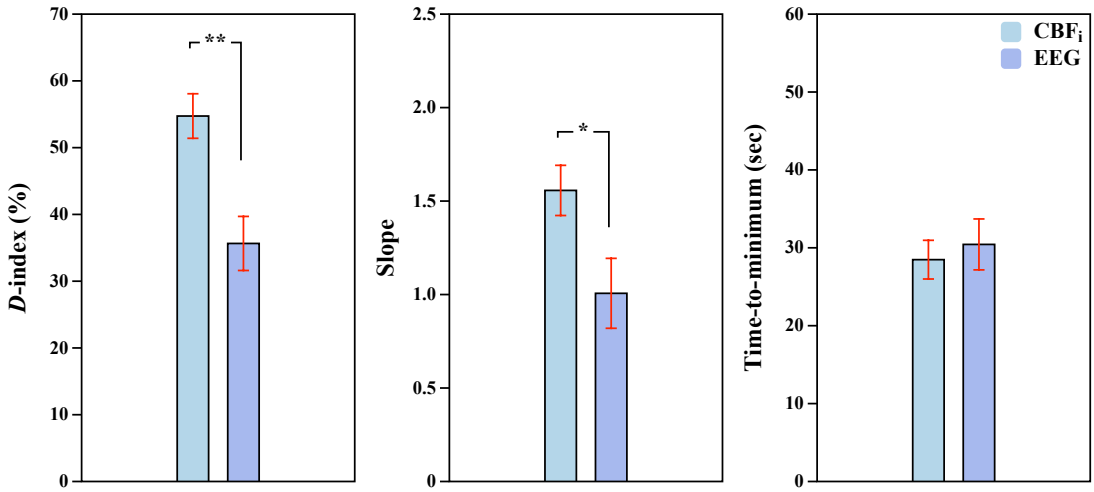

Figure 4.3. The comparison of *D*-index, slope, and time-to-minimum between CBF_i and EEG power spectra in all patients. * $P < 0.05$ and ** $P < 0.001$. All data are represented in mean ± SEM.

Considering the literature, patients were divided into three groups with respect to the degree of EEG *D*(t) changes as more than 50% changes (group A), between 25–50% (group B), and less than 25% (group C). Figure 4.4 demonstrates a time course of *D*(t) of EEG and CBF_i based on this classification.

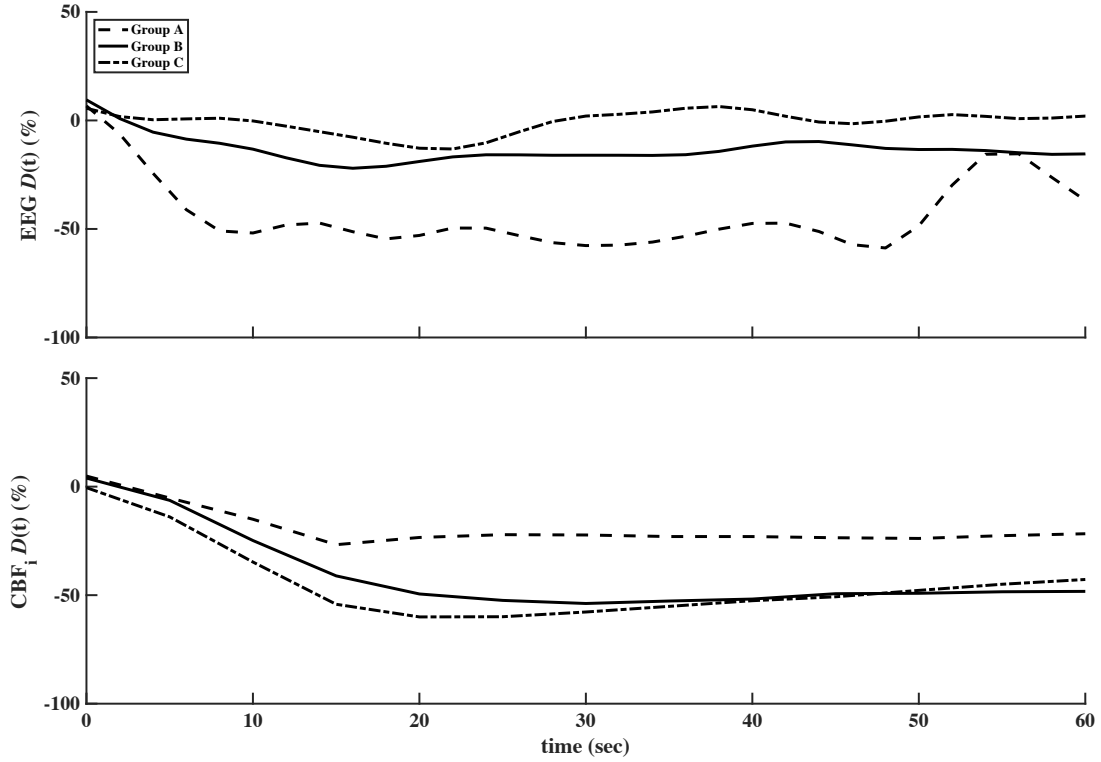

Figure 4.4. Desynchronization function time course of EEG power spectra (top panel) and CBF_i (bottom panel) in three groups. The groups were established according to the degree of decrease in EEG. Group A indicates major EEG changes (dashed line), group B indicates moderate EEG changes (straight line), and group C (dashed dot line) indicates no EEG changes.

In group A (#12, 14, and 22), the Mann-Whitney U test revealed that the *D*-index of CBF_i (median = 26%) was significantly lower than that of EEG (63%, $P = 0.05$). The slope of EEG ($S = 2.4$) was significantly a faster decrease than CBF_i ($S = 0.72$, $P = 0.05$). There were no statistically significant differences between CBF_i and EEG in any group A for time-to-minimum (Figure 4.5).

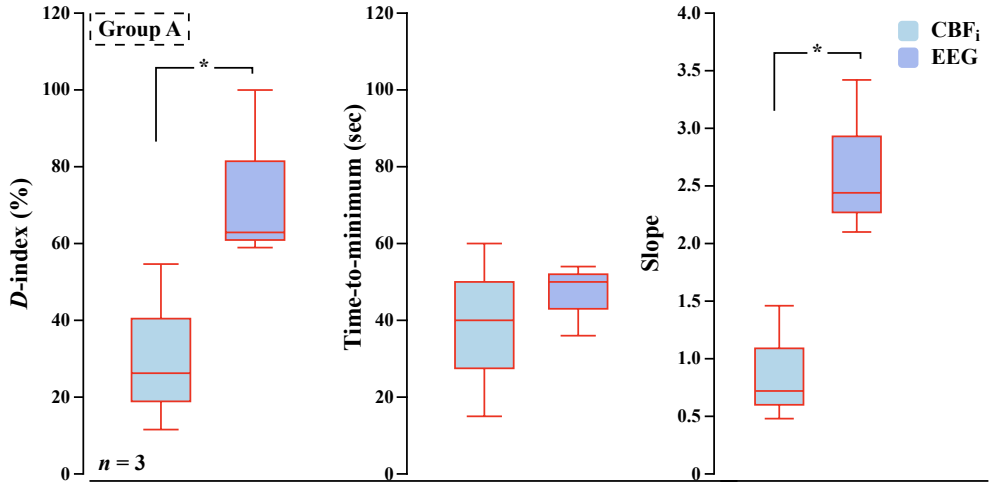

Figure 4.5. The comparison of *D*-index, time-to-minimum, and slope between CBF_i and EEG power spectra in group A. * $P < 0.05$. All data are represented in a whisker plot.

In group B (#3, 4, 5, 7, 9, 10, 11, 13, 15, 16, 17, 18, 19, 20, and 23), *D*-index of CBF_i (56%) was significantly higher than EEG (34%, $P = 0.05$). In addition, CBF_i ($S = 1.7$) decrease significantly faster than EEG ($S = 0.8$, $P = 0.002$). There were no statistically significant differences between CBF_i and EEG in any group B for time-to-minimum (Figure 4.6).

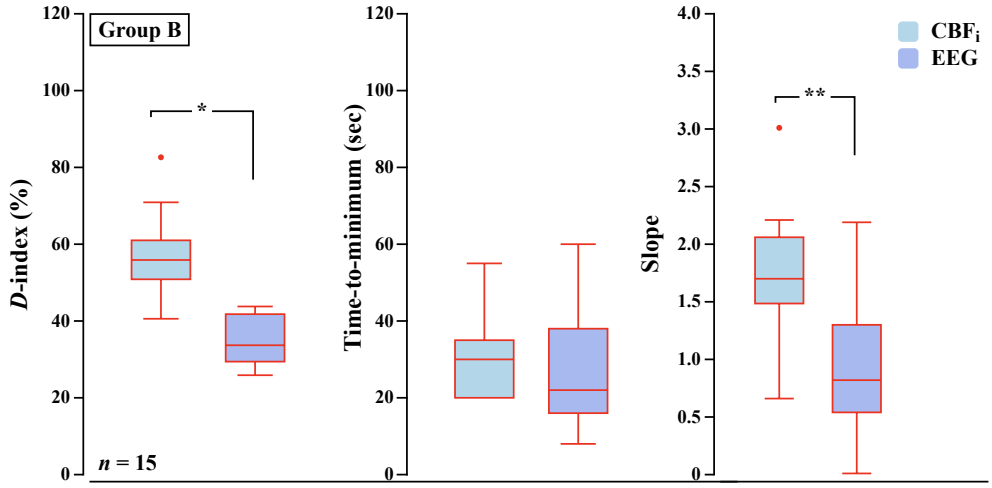

Figure 4.6. The comparison of *D*-index, time-to-minimum, and slope between CBF_i and EEG power spectra in group B. * $P < 0.05$ and ** $P < 0.001$. All data are represented in a whisker plot.

In group C (#1, 2, 6, 8, and 21), the *D*-index of CBF_i (69%) was significantly higher than EEG (15%, $P = 0.009$). Although CBF_i ($S = 1.8$) decrease faster than EEG ($S = 0.2$), there was no significant differences ($P = 0.08$). There were no also statistically significant differences between CBF_i and EEG in any group C for time-to-minimum (Figure 4.7).

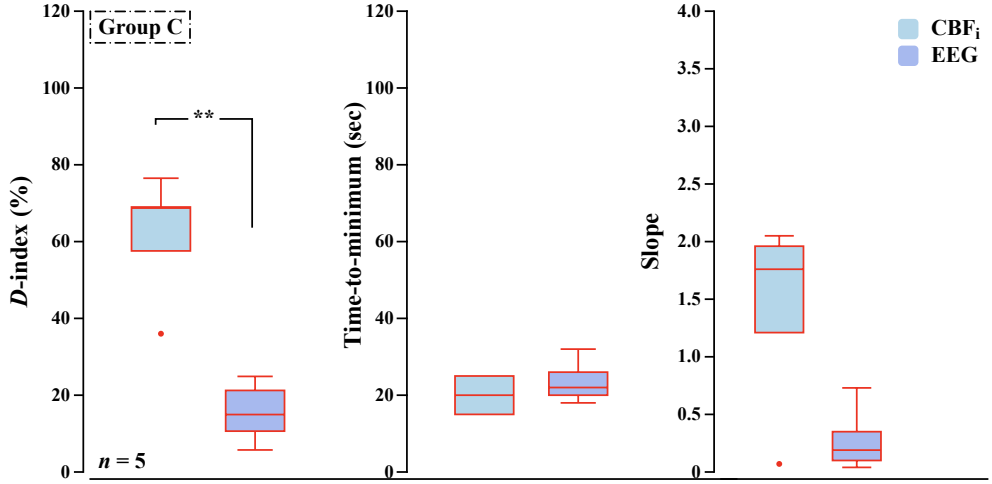

Figure 4.7. The comparison of *D*-index, time-to-minimum, and slope between CBF_i and EEG power spectra in group C. ** $P < 0.001$. All data are represented in a whisker plot.

4.3. CBF_i and EEG Changes in Different Anesthetic Agents

Figure 4.8 demonstrates a time course of *D*(t) of EEG and CBF_i with respect to the anesthetic agent used for induction.

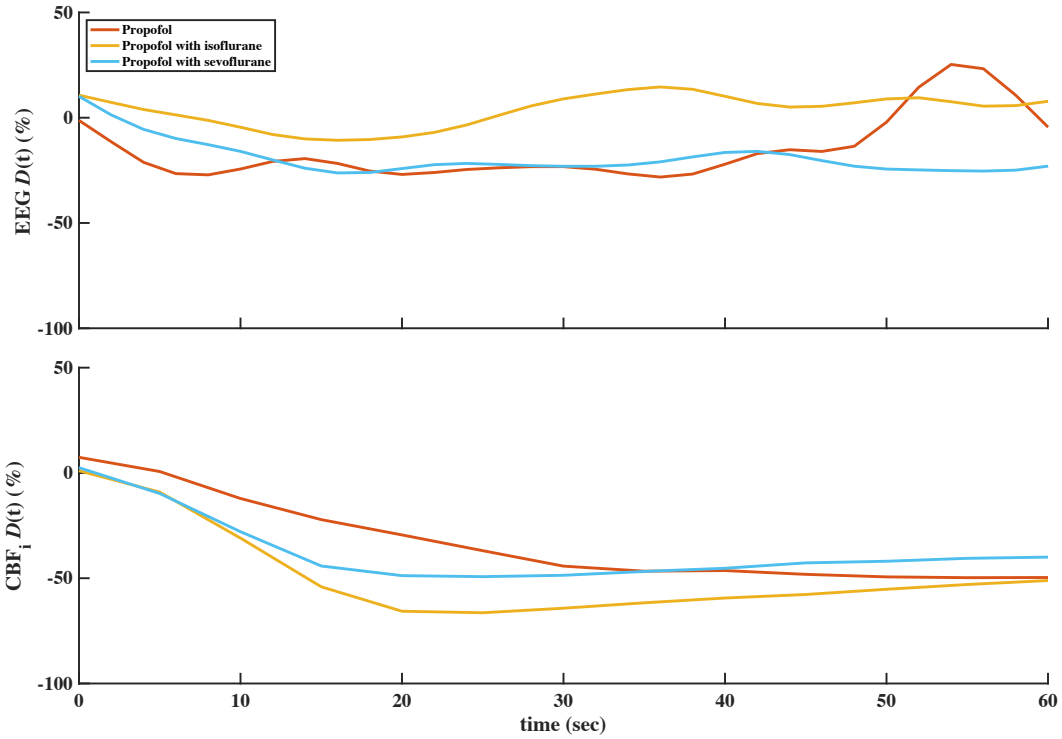

Figure 4.8. Desynchronization function time course of EEG power spectra (top panel) and CBF_i (bottom panel) with respect to induction anesthesia. The crimson color indicates propofol, brown indicates propofol with isoflurane, and turquoise indicates propofol with sevoflurane.

Within EEG spectral power, there were no significant differences between anesthetic agents for *D*-index ($F_{2,20}$ = 2.9, P = 0.08, Figure 4.9A right), slope ($F_{2,20}$ = 1.9, P = 0.18, Figure 4.9B right), and time-to-minimum ($F_{2,20}$ = 1.7, P = 0.2, Figure 4.9C right). There were no significant differences within CBF_i for *D*-index ($F_{2,20}$ = 1.5, P = 0.2, Figure 4.9A left) and slope ($F_{2,20}$ = 1.1, P = 0.4, Figure 4.9B left). The time-to-minimum significantly differed between anesthetics agents for CBF_i ($F_{2,20}$ = 0.9, P = 0.001, Figure 4.9C left). A Tukey post hoc test revealed that the time-to-minimum of CBF_i under propofol alone (46 ± 7 sec) was significantly longer than that of propofol with sevoflurane (25 ± 2 sec, P = 0.001) and propofol with isoflurane (23 ± 1 sec, P = 0.003).

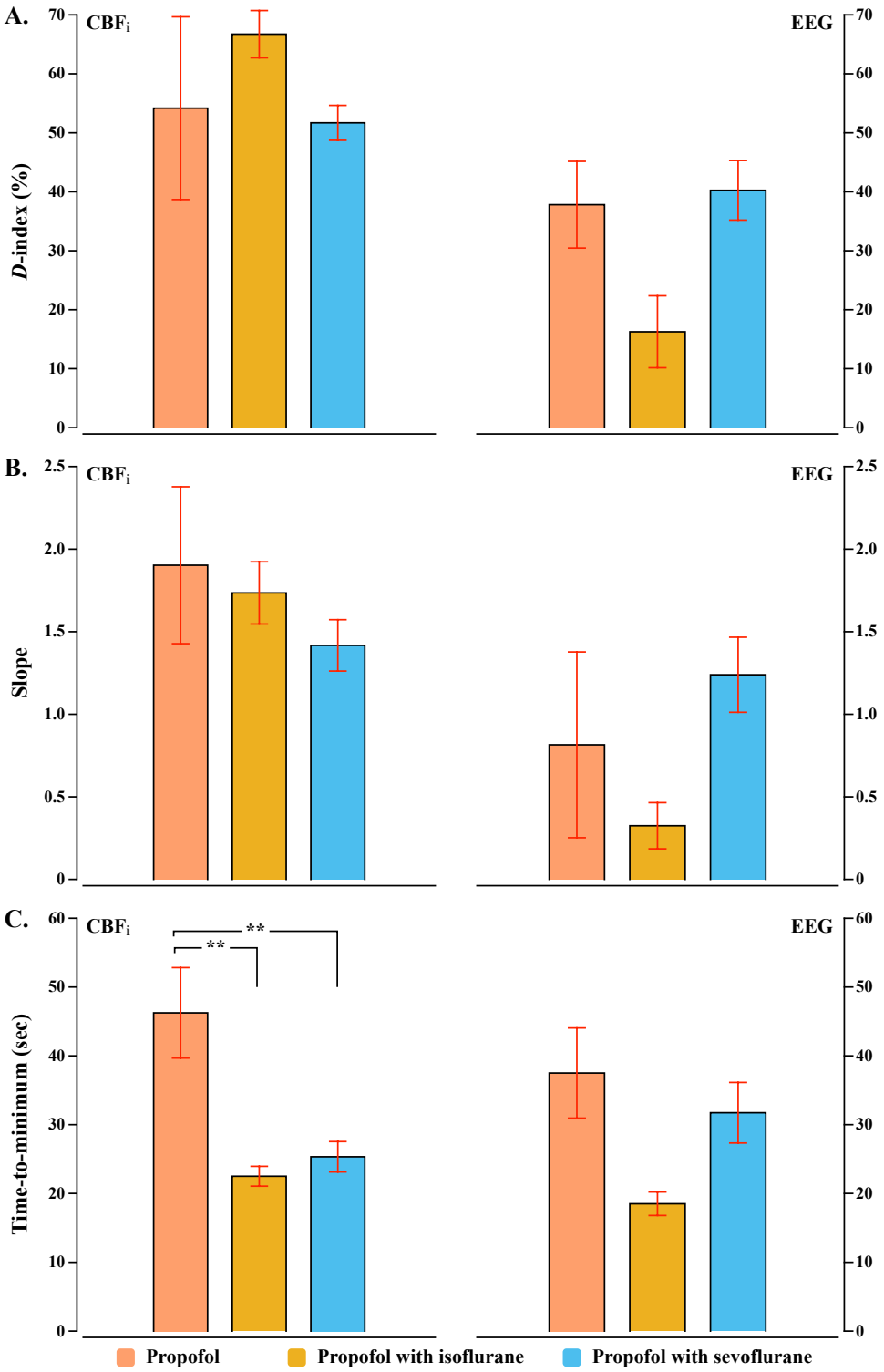

Figure 4.9. The *D*-index (A), slope (B), and time-to-minimum (C) results of CBF_i (left) and EEG power spectra (right) in each induction anesthesia. The crimson color indicates propofol, brown indicates propofol with isoflurane, and turquoise indicates propofol with sevoflurane. All data are represented in mean ± SEM. ** $P < 0.001$.

Further, comparing CBF_i and EEG D(t) showed significant differences in anesthetic agents. The Mann-Whitney U test revealed that the D-index of CBF_i was significantly higher than EEG spectral power under propofol with sevoflurane (median, IQR – CBF_i = 53, 12% and EEG = 34, 14%, P = 0.007, Figure 4.10A right) and propofol with isoflurane (CBF_i = 66, 16% and EEG = 13, 22%, P = 0.02, Figure 4.10A middle). However, there were no significant differences in the D-index of CBF_i and EEG under propofol (P = 0.4, Figure 4.10A left).

For slope, there was a significant difference under propofol with isoflurane where CBF_i (median, IQR– S = 2, 0.7) decreased faster than EEG power spectra (S = 0.2, 0.5, P = 0.02, Figure 4.10B middle). There were no statistical slope differences between CBF_i and EEG spectral power under propofol (P = 0.2, Figure 4.10B left) and propofol with sevoflurane (P = 0.4, Figure 4.10B right).

There were no statistical differences between CBF_i and EEG spectral power for time-to-minimum in any anesthetic agents (P = 0.6 for propofol, P = 0.1 for propofol with isoflurane, and P = 0.4 for propofol with sevoflurane, Figure 4.10C, respectively).

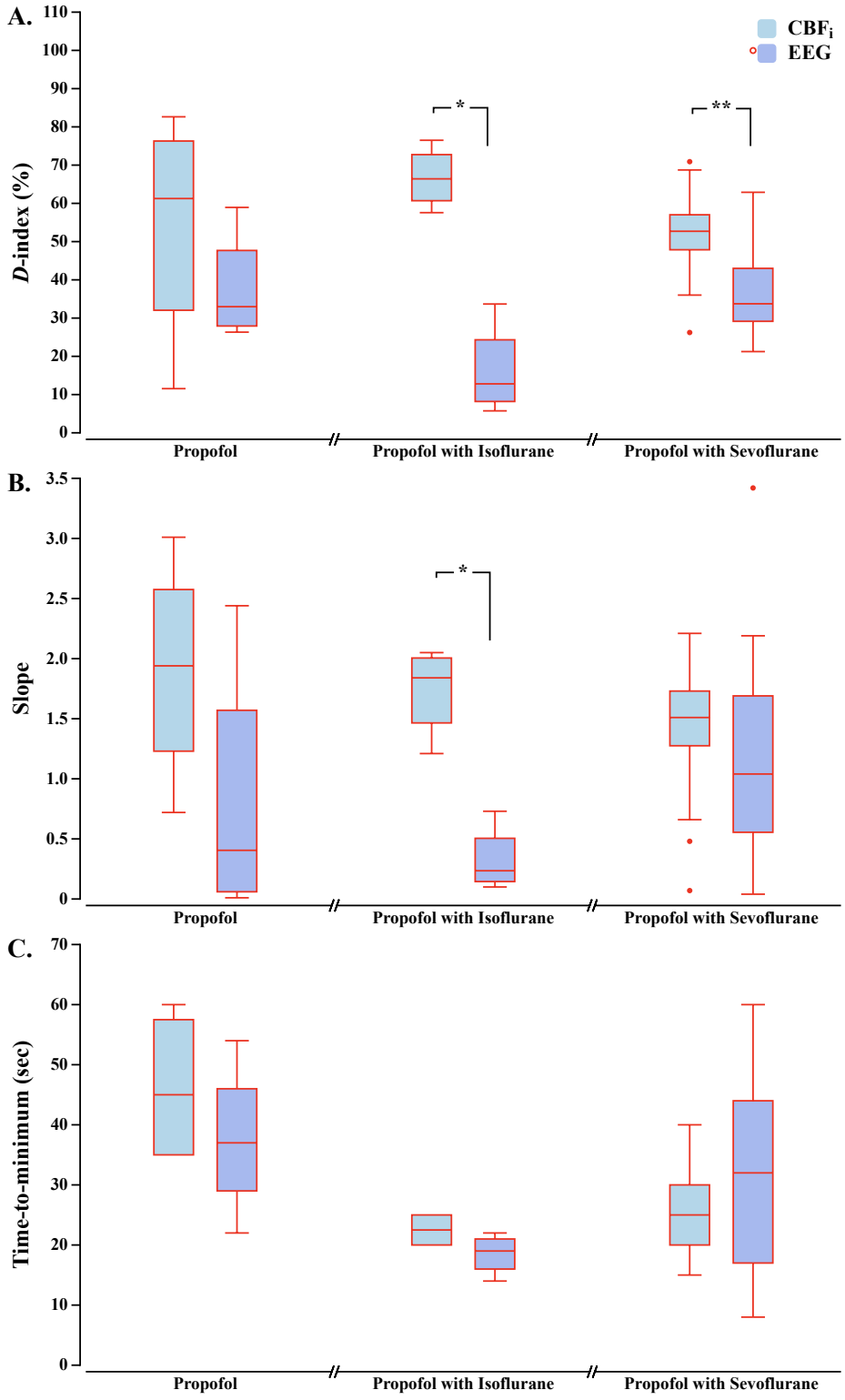

Figure 4.10. The *D*-index (A), slope (B), and time-to-minimum (C) comparison between CBF_i (cyan) and EEG power spectra (purple) in each induction anesthesia. * $P < 0.05$ and ** $P < 0.001$. All data are represented in a whisker plot.

4.4. Variations in Hemispheric CBF_i and EEG Power Spectra

Table 4.2 indicates hemispheric variations for CBF_i and EEG and Figure 4.11 demonstrates typical hemispheric CV results of CBF_i and EEG power spectra from patient #21.

Table 4.2. The results of hemispheric CV for CBF_i and EEG power spectra in each patient. All data are represented in percentages.

Patient	CBF_i		EEG	
	CV^{ipsi} (%)	CV^{contra} (%)	CV^{ipsi} (%)	CV^{contra} (%)
1	2	NA	100	102
2	1	NA	67	66
3	2	NA	83	82
4	1	NA	111	115
5	2	NA	59	57
6	2	NA	48	47
7	2	NA	82	84
8	2	2	81	82
9	2	3	62	62
10	1	3	69	75
11	2	3	65	64
12	3	5	64	68
13	3	4	90	92
14	2	4	69	67
15	3	1	83	86
16	7	6	83	92
17	4	4	110	114
18	4	8	64	64
19	4	2	73	75
20	1	1	102	101
21	3	2	45	50
22	4	8	52	52
23	4	4	67	66

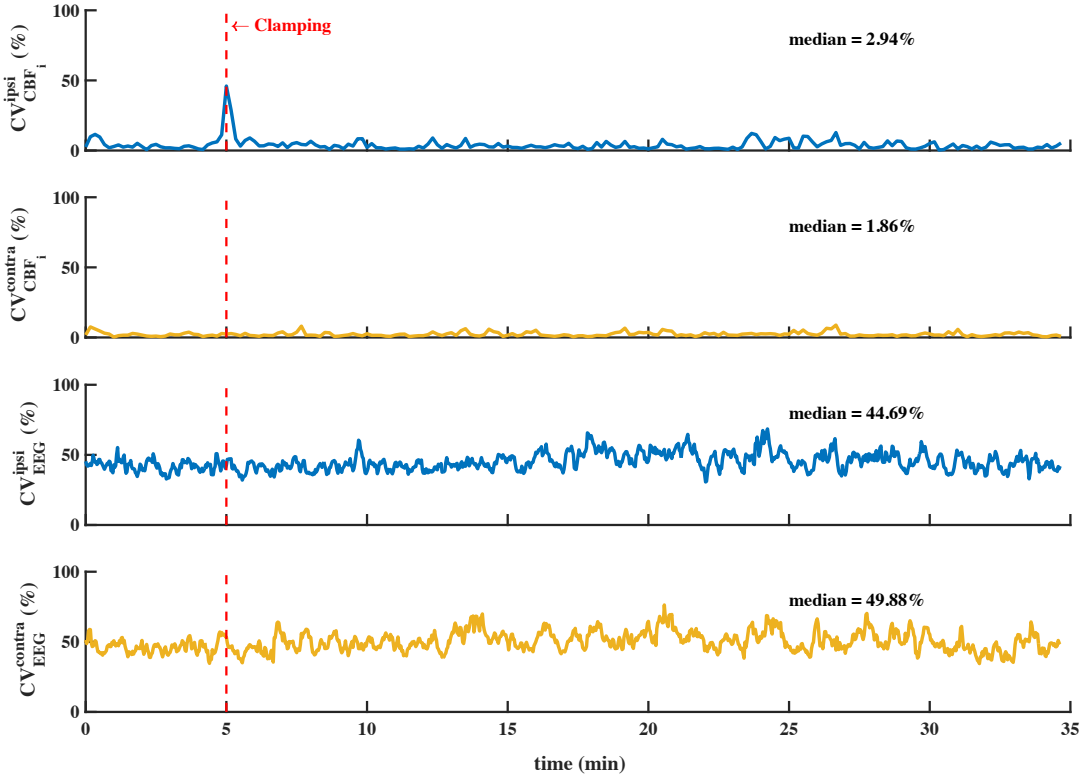

Figure 4.11. A typical time course of hemispheric CV results from a patient (#21). Panels one and two indicate CV of ipsilateral and contralateral CBF_i, respectively. Panels three and four indicate CV of ipsilateral and contralateral EEG power spectra, respectively. Ipsilateral and contralateral responses are demonstrated in blue and brown, respectively.

There was less variation in ipsilateral EEG (75 ± 4%) than that of contralateral (77 ± 4%, $t_{44} = -0.27$, $P = 0.8$, Figure 4.12 right). In addition, although there was more variation for hemispheric CBF_i (CV^{ipsi} = 3 ± 0.3% and CV^{contra} = 4 ± 0.5%), there were no statistical differences ($t_{44} = -1.9$, $P = 0.06$, Figure 4.12 left).

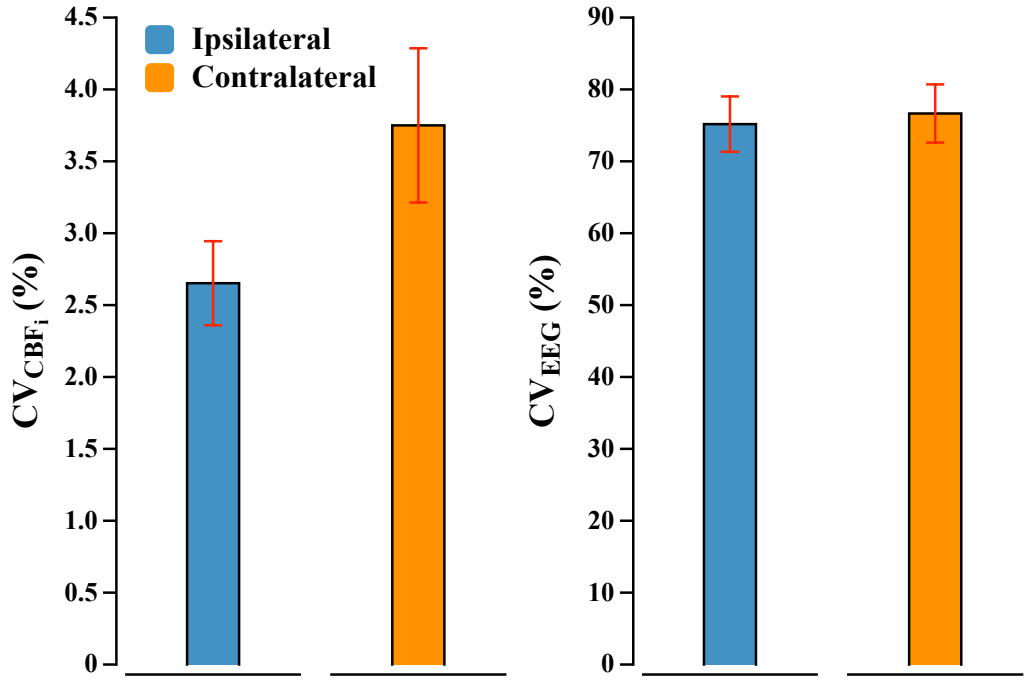

Figure 4.12. The differences between ipsilateral (blue) and contralateral (orange) CV within CBF_i (left) and EEG power spectra (right) responses. All data are represented in mean ± SEM.

The $CV_{CBF_i}^{ipsi}$ significantly differed between anesthetic agents ($F_{2,20}$ = 8.2, P = 0.002). A Tukey post hoc test revealed that there were more variations in $CV_{CBF_i}^{ipsi}$ under propofol anesthesia (4.5 ± 0.9%) than propofol with sevoflurane (2.5 ± 0.3%, P = 0.009) and propofol with isoflurane (1.5 ± 0.3%, P = 0.002, Figure 4.13A left). In addition, there were no significant differences for $CV_{CBF_i}^{contra}$ for any anesthetic agents ($F_{2,13}$ = 2.2, P = 0.15, Figure 4.13A right). There were also no significant differences for CV_{EEG}^{ipsi} ($F_{2,20}$ = 1.2, P = 0.3) and CV_{EEG}^{contra} ($F_{2,20}$ = 1.3, P = 0.3) for any anesthetic agents (Figure 4.13B).

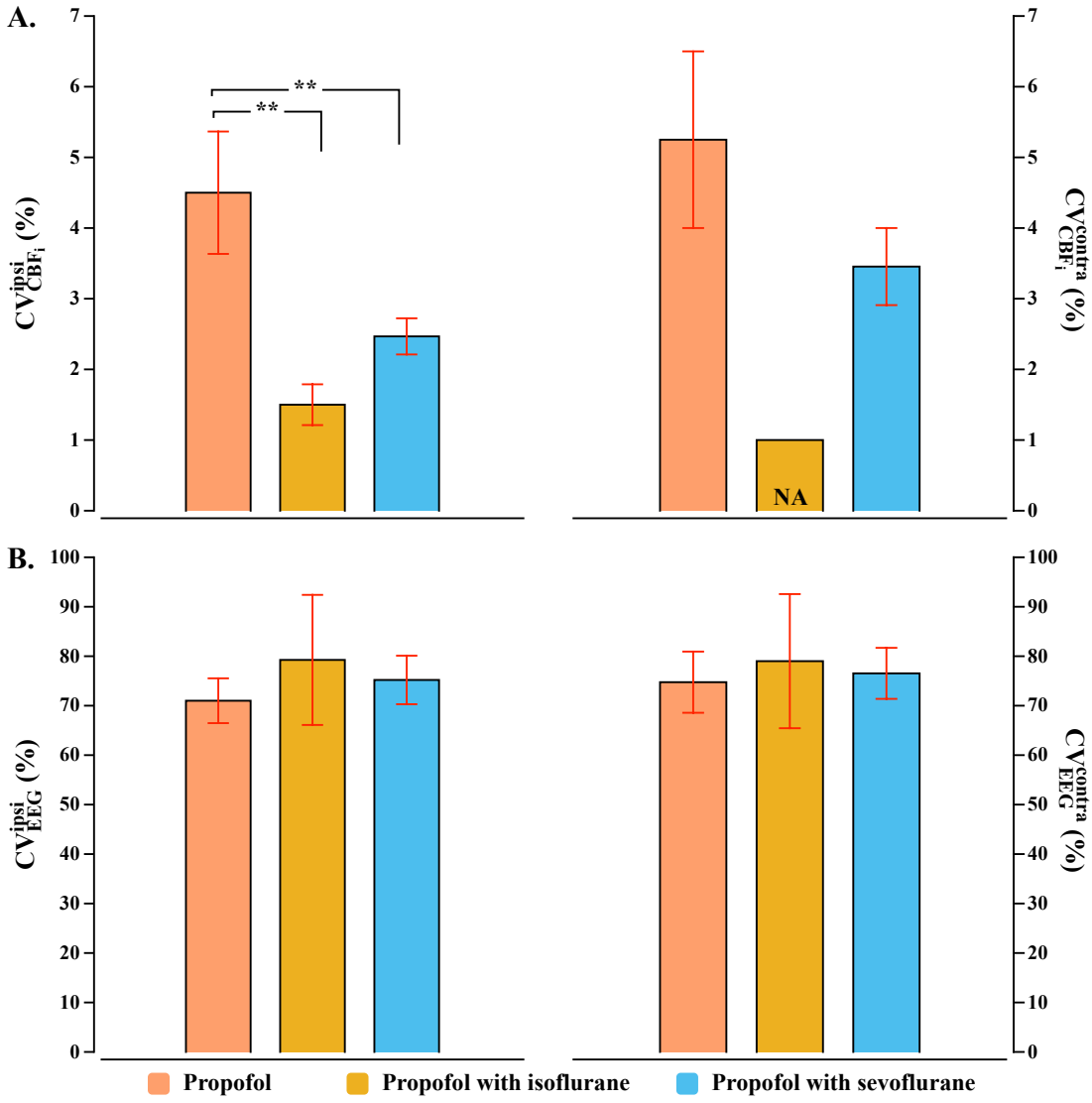

Figure 4.13. The variation results of $CV_{CBF_i}^{ipsi}$ (A left), $CV_{CBF_i}^{contra}$ (A right), CV_{EEG}^{ipsi} (B left), and CV_{EEG}^{contra} (B right) in each induction anesthesia. The crimson color indicates propofol, brown indicates propofol with isoflurane, and turquoise indicates propofol with sevoflurane. There was only one data point for $CV_{CBF_i}^{contra}$, and thus statistical analysis could not be performed. All data are represented in mean ± SEM. ** $P < 0.001$.

4.5. Perioperative Complications

Patients tolerated the procedure well, and their entire operative course remained neurologically intact, with no signs of transient ischemic attack (TIA) or stroke. However, the postoperative period of some patients was notable for mild headache, hypotension, or hypertension. During the postoperative course, these symptoms were resolved without issues. In two patients (#4 and #12), there was a weakness in the left lower extremity. There were also postoperative transient neurological changes in two patients (#4 and #23) with slightly asymmetric smiles. The weakened smile is often induced by bupivacaine that is injected with the incision and can last 24 hours. However, these symptoms improved throughout the patient's stay, and the patients were discharged in stable condition with no new neurologic deficits. Furthermore, 30–day follow-ups of our patients reported no sign of symptoms of TIA or stroke. Additionally, their blood pressure was well controlled.

5. DISCUSSION

In this dissertation, we demonstrated the feasibility of noninvasive cerebral hemodynamic monitoring via a combined DCS-NIRS system and also utilized these measurements with clinically acquired EEG measurements. Indeed, monitoring neuronal and neurovascular responses can help the clinical team to establish better inpatient management, and therefore achieve optimal perfusion for CEA patients.

We also compared changes in the desynchronization function of CBF_i and EEG as we hypothesized that there might be notable differences between neuronal and neurovascular responses. We addressed this hypothesis in two ways. To begin with, we categorized patients with respect to well-established EEG spectral criteria. Accordingly, patients were divided into three groups based on major, moderate, and no EEG spectral changes. Then, we compared these EEG spectra changes with CBF_i since some anesthetic agents may trigger flow-metabolism coupling or decoupling. For further investigation, we divided patients into three groups with respect to the anesthesia used for induction and compared outcomes of desynchronization function to elucidate responses in CBF_i and EEG power spectra. Thus, we indicated anesthesia-induced differences for CBF_i and EEG power spectra due to tight coupling. Subsequently, we captured clamp-induced variations for CBF_i and EEG in each hemisphere and then detailed these variations with reference to each induction anesthesia.

5.1. Intraoperative Neuromonitoring during CEA

Under local anesthesia, the clinical team can delineate the patient's condition by performing simple arithmetic tasks or asking the patient to rotate the extremities contralateral to the surgical side since they can maintain verbal communication (7,80). Consequently, the shunt utilization can be decided based on an intraoperative assessment to restore arterial inflow to the ipsilateral cerebral hemisphere. However, the decision of whether to utilize a shunt is more challenging under general anesthesia (81–83). Since shunt utilization accompanies a low incidence of carotid intimal injury and can encumber exposure, some surgeons evade routine shunt insertion. Fortunately,

there are several neuromonitoring techniques so that shunt utilization can be decided intraoperatively based on the patient's condition under general anesthesia (84). Nonetheless, there is no proper neuromonitoring technique to examine optimal cerebral perfusion, and the ideal method remains debatable (37).

To summarize, most of the available neuromonitoring techniques offer indirect measures of cerebral perfusion (e.g., EEG, SSEP, and NIRS). Among them, NIRS can indicate oxygen saturation changes with respect to carotid clamping or stent insertion (85) since a decrease in oxygen saturation was correlated with postoperative neurologic deficits. This was also demonstrated for CEA patients by other neuromonitoring techniques such as EEG, TCD ultrasound, and CSP (37,82,86–88). In addition, NIRS also showed comparable sensitivity (30–80%) and specificity (77–98%) results during CEA, which were also achieved by other monitoring techniques (89–91).

EEG is an easy-to-use and feasible neuromonitoring technique, though it has several limitations. EEG readings rely on expert neurophysiologists to interpret raw and processed data. However, each has constraints and trade-offs over another. The raw data is noisy due to other devices in the operation room. Moreover, some patients developed neurological deficits and indicated clinically significant cerebral ischemia even though EEG maintains unaltered (92). While processed EEG presents readability, conversion might lead to the loss of considerable information. One method is density spectral array analysis, which facilitates smooth interpretation of EEG. Still, it might not reliably indicate cerebral ischemia (9). Another is compressed spectral array analysis, although it is less sensitive than the raw EEG to detect cerebral ischemia (8).

This is where optical neuromonitoring techniques step in. Over the past decades, optical neuromonitoring techniques have made remarkable progress in providing easy-to-use, reliable, and noninvasive devices to enlighten the underpinnings of cerebral physiology during surgeries. Since DCS is sensitive to blood flow, intraoperative monitoring of clamp-induced hypoperfusion or unclamp-induced hyperperfusion would significantly contribute to inpatient care (75,78,93,94). As we demonstrated with this dissertation study, the additional perfusion index provided by DCS to NIRS and EEG offers a complementary assessment of cerebral physiology.

5.2. Intraoperative Neuronal and Neurovascular Changes

Clamping caused marked changes in ipsilateral CBF_i, Δ[HbO], Δ[HbR], and EEG power spectra. There was a steep drop of CBF_i and Δ[HbO] and a slight increase in Δ[HbR] due to transient interruption of perfusion. This reduction in perfusion due to clamping triggers an increase of blood volume (Δ[HbO] + Δ[HbR]) and caused a partial recovery of CBF_i. Conversely, unclamping caused a marked overshoot of CBF_i and Δ[HbO] while causing a drop of Δ[HbR] (Figure 4.1A–C, respectively). There were also changes in the contralateral hemisphere due to clamping and unclamping. Medically elevated MAP at clamping caused a contralateral increase of blood volume and CBF_i which also contributed to the aforementioned recovery to the ipsilateral CBF_i due to vascular pressure differences (Figure 4.1A, D, respectively). Upon unclamping, there was a decrease of contralateral CBF_i and Δ[HbO] due to gradual recovery of vascular pressure since MAP was medically reduced (Figure 4.1A, B, respectively).

The desynchronization function is a useful analysis method to quantify spectral changes in alpha band power in relation to CBF_i. We found that the minimum value (*D*-index) of CBF_i was significantly higher than spectral EEG (Figure 4.3 left). This is expected since neuronal activity depends on blood flow and transient blood flow cessation due to clamping may trigger a slower reduction in EEG power spectra. This was confirmed with slope results. The decrease in CBF_i was significantly faster than EEG power spectra as we demonstrated with slope changes (Figure 4.3 middle). This implies that the changes in EEG power spectra are slower in response to a reduction in CBF_i, although the time of these changes was not significantly differed between them (Figure 4.3 right). These results were similar to those that employed the same methodology between CBF_i and spectral EEG (27).

However, there were different responses between CBF_i and EEG power spectra when patients are grouped with respect to robust spectral EEG criteria. Patients with moderate and no spectral changes showed significantly higher CBF_i *D*-index than EEG power spectra (Figure 4.6 and 4.7 left, respectively), whereas patients with major spectral changes showed significantly lower CBF_i *D*-index than EEG power spectra (Figure 4.5 left). Moreover, patients with major spectral changes had a significantly faster reduction in EEG power spectra (Figure 4.5 right) whilst patients with moderate

spectral changes had a faster reduction in CBF_i (Figure 4.6 right). Potentially severe EEG changes may occur due to pre-existing subcortical ischemia and therefore clamping might superimpose with previous electrophysiologic anomalies, resulting in such differences between CBF_i and spectral EEG (95). Likewise, CBF_i changes might be more notable in the prefrontal cortex than spectral EEG from the whole hemisphere. As we acquired optical data from the prefrontal area, clamp-induced changes may be more evident in CBF_i than in hemispheric spectral EEG since decrements of CBF_i is different throughout the hemisphere. Nevertheless, many factors could lead to these differences between CBF_i and spectral EEG such as bilateral stenosis, comorbid diseases, smoking status, intraoperative MAP management, heart rate, anesthetics for induction and maintenance, and cerebral adaptive capacity.

5.3. Neuronal and Neurovascular Changes in Anesthetic Agents

Probably the most critical question is how anesthetic agents affect CBF and cerebral metabolism. Indeed, each anesthetic agent used for induction or maintenance diminishes cerebral metabolism. Currently, no reliable data indicates specific advantages of one anesthesia over the other (96). It has been proposed that sevoflurane produces less vasodilation in general while offering instantaneous recovery (48). Though, different concentrations of sevoflurane produce different changes in CBF and cerebral metabolism. In addition, higher sevoflurane concentrations also produce flow-metabolism decoupling and reduce ipsilateral ICA pressure more than that of contralateral (97). Propofol causes an evident reduction in CBF and cerebral metabolism although higher propofol concentrations resulted in further hemodynamic stability (6,49,98). Isoflurane poses fewer EEG changes and reduces CBF with respect to clamping (99). Nevertheless, these anesthetic agents pose a degree of neuroprotection (100–102). Additionally, it has been proposed that hemodynamic stability can be improved with opioids, including fentanyl and its derivatives (103).

In a similar line with the literature, we found relatively the same reduction in CBF_i and spectral EEG for propofol alone and propofol with sevoflurane (Figure 4.9A). However, we found less spectral EEG changes and more reduced CBF_i *D*-index for propofol with isoflurane (Figure 4.9A). We found no significant differences within

spectral EEG for any induction anesthesia. However, although there were no significant differences in *D*-index and slope within CBF_i (Figure 4.9A, B, respectively), the time of *D*-index was significantly longer in propofol than propofol with sevoflurane and propofol with isoflurane (Figure 4.9C). This can be explained by the neuroprotective effect of propofol, allocating greater hemodynamic stability than others as proposed in the literature.

We also compared CBF_i and spectral EEG under the same anesthetic agent. There were no significant differences between CBF_i and spectral EEG under propofol for *D*-index, slope, and time-to-minimum (Figure 4.10A–C left, respectively). Since isoflurane produces less EEG changes than CBF_i, we found a significantly higher *D*-index in CBF_i than in spectral EEG (Figure 4.10A middle). Moreover, the reduction in CBF_i was significantly faster than spectral EEG only under propofol with isoflurane anesthesia (Figure 4.10B middle). The *D*-index was also significantly higher in CBF_i than EEG for propofol with sevoflurane (Figure 4.10A right), which can be explained by the vasodilation induced by sevoflurane. There were no other significant differences between CBF_i and spectral EEG. This might be because all these anesthetic agents offer rapid recovery and a degree of neuroprotection.

5.4. Clamp-induced Hemispheric Variations

Overall, there were no significant hemispheric variations for averaged CBF_i or spectral EEG (Figure 4.12). However, while there were no significant differences in *D*-index within CBF_i with respect to anesthetic agents (Figure 4.9A left), there were large variations in ipsilateral CBF_i (Figure 4.13A left). We detected significantly increased ipsilateral CBF_i signal variability in propofol than in other anesthetic agents. It can be suggested that physiological cardiopulmonary pulsations can influence cerebral hemodynamics more under propofol anesthesia. Therefore, it can be hypothesized that propofol offers more hemodynamic integrity as it distinguishes from other anesthetic agents by showing significantly large variations in the ipsilateral CBF_i. However, we acknowledge that this is a big statement, requiring further validation.

5.5. Significance of Multimodal Approach

EEG measurements are important with respect to estimating cerebral ischemia under general anesthesia regardless of its limitations. However, it is hard to purely rely on EEG for assessing cerebral physiology since the EEG waves oscillate differently under local and general anesthesia even with different chemical or volatile anesthetics. Several attempts to replace the EEG with another neuroimaging modality could not find a robust place in clinical practice. This depends on several reasons such as feasibility, robustness, and not interfering with the surgical area. Even though EEG provides important insight into neurophysiology as a surrogate measure of CBF, a multi-modal approach for measuring cerebral perfusion is necessary. Therefore, we believe that a combined DCS-NIRS system and EEG extensively address every requirement of assessing cerebral physiology under general anesthesia during CEA.

5.6. Limitations

We are intrinsically limited by NIRS and DCS, as our model assumes consistent head anatomy and no extracerebral interference differences across patients. One limitation of our study is the small number of patients enrolled for CBF_i-NIRS and spectral EEG comparisons between anesthetic agents. Another limitation of our study is the assumption of the same optical properties among all patients. These limitations may contribute to the inter-subject variability in CBF_i, Δ[HbO], and Δ[HbR]. Considering the small number of patients enrolled for propofol and propofol with isoflurane in this study, it is not possible to state whether the desynchronization function can be distinguished between CBF_i and spectral EEG. We are also limited by the dose and exact application time of anesthetics for maintenance during the intraoperative course as it differs patient by patient. Nevertheless, most of our patients showed similar hemodynamic trends throughout the CEA procedure.

6. CONCLUSION and FUTURE PERSPECTIVE

In conclusion, a combined optical DCS-NIRS system can provide important insight into cerebral hemodynamics during CEA, preventing undesirable events in ischemia-sensitive organs such as the brain. Since DCS is sensitive to changes in blood flow, it can be very useful to pose cerebral hypoperfusion which can lead to neurophysiologic dysfunctions and potential neuronal cell death. In addition, DCS requires neither online visual inspection nor offline power spectral analysis since it is more sensitive to determine CBF changes than EEG. This can potentially allow early detection of cerebral hypoperfusion and concomitantly brain injury. Moreover, by monitoring CBF_i and EEG-derived indices, we showed a comprehensive assessment of cerebral physiology during CEA. Thus, we conclude that DCS alone or combined with NIRS can provide a complementary cerebral hemodynamic assessment to EEG during surgery, which can potentially guide the clinical team to mitigate perioperative stroke and neurological injury by determining personalized perfusion strategies. Nevertheless, further studies are needed in order for demonstrating the strength of CBF_i and EEG under different combinations of anesthetic regimens.

What remains to be understood is the reperfusion with unclamping and effects on CBF_i and spectral EEG under specific anesthesia. Therefore, we consider applying advanced algorithms to disentangle the multimodality of our data sets, such as multimodal source power correlation analysis or temporally embedded canonical correlation analysis. This will allow us to consider physiological variations, including MAP and superficial blood and metabolism.

7. REFERENCES

1. Howell SJ. Carotid endarterectomy. Bja Br J Anaesth. 2007;99(1):119–31.
2. Romero JR, Pikula A, Nguyen TN, Nien YL, Norbash A, Babikian VL. Cerebral Collateral Circulation in Carotid Artery Disease. Curr Cardiol Rev. 2009;5(4):279–88.
3. Vrselja Z, Brkic H, Mrdenovic S, Radic R, Curic G. Function of Circle of Willis. J Cereb Blood Flow Metabolism. 2014;34(4):578–84.
4. Cursi M, Meraviglia MV, Fanelli GF, Chiesa R, Tirelli A, Comi G, et al. Electroencephalographic background desynchronization during cerebral blood flow reduction. Clin Neurophysiol. 2005;116(11):2577–85.
5. Rowed DW, Houlden DA, Burkholder LM, Taylor AB. Comparison of Monitoring Techniques for Intraoperative Cerebral Ischemia. Can J Neurological Sci. 2004;31(3):347–56.
6. Kaisti KK, Långsjö JW, Aalto S, Oikonen V, Sipilä H, Teräs M, et al. Effects of Sevoflurane, Propofol, and Adjunct Nitrous Oxide on Regional Cerebral Blood Flow, Oxygen Consumption, and Blood Volume in Humans. Anesthesiology. 2003;99(3):603–13.
7. Monnig A, Budhrani G. Anesthesiology, A Practical Approach. 2018;645–55.
8. Hanowell LH, Soriano S, Bennett HL. EEG power changes are more sensitive than spectral edge frequency variation for detection of cerebral ischemia during carotid artery surgery: A prospective assessment of processed EEG monitoring. J Cardiothor Vasc An. 1992;6(3):292–4.
9. Kearse LA, Martin D, McPeck K, Lopez-Bresnahan M. Computer-derived density spectral array in detection of mild analog electroencephalographic ischemic pattern changes during carotid endarterectomy. J Neurosurg. 1993;78(6):884–90.
10. Sloan TB. Anesthetic Effects on Electrophysiologic Recordings. J Clin Neurophysiol. 1998;15(3):217–26.
11. Jansen C, Vriens EM, Eikelboom BC, Vermeulen FE, Gijn J van, Ackerstaff RG. Carotid endarterectomy with transcranial Doppler and electroencephalographic monitoring. A prospective study in 130 operations. Stroke. 2018;24(5):665–9.
12. Kaya K, Zavriyev AI, Orihuela-Espina F, Simon MV, LaMuraglia GM, Pierce ET, et al. Intraoperative cerebral hemodynamic monitoring during carotid endarterectomy via diffuse correlation spectroscopy and near-infrared spectroscopy. Brain Sci. 2022;12(8):1025.
13. Zavriyev AI, Kaya K, Farzam P, Farzam PY, Sunwoo J, Jassar AS, et al. The role of diffuse correlation spectroscopy and frequency-domain near-infrared spectroscopy in monitoring cerebral hemodynamics during hypothermic circulatory arrests. JTCVS Techniques. 2021;(7):161–77.
14. Mazziotti R, Scaffei E, Conti E, Marchi V, Rizzi R, Cioni G, et al. The amplitude of fNIRS hemodynamic response in the visual cortex unmasks autistic traits in typically developing children. Transl Psychiat. 2022;12(1):53.
15. Abdalmalak A, Milej D, Norton L, Debicki DB, Owen AM, Lawrence KS. The Potential Role of fNIRS in Evaluating Levels of Consciousness. Frontiers in human neuroscience. 2021;15:703405.
16. Delpy DT, Cope M, Zee P van der, Arridge S, Wray S, Wyatt J. Estimation of optical pathlength through tissue from direct time of flight measurement. Physics in Medicine & Biology. 1988;33:1433.
17. Yucel MA, Selb JJ, Huppert TJ, Franceschini MA, Boas DA. Functional Near Infrared Spectroscopy: Enabling Routine Functional Brain Imaging. Curr Opin Biomed Eng. 2017;4:78–86.

18. Nair VV, Kish BR, Yang HC (Shawn), Yu Z, Guo H, Tong Y, et al. Monitoring anesthesia using simultaneous functional Near Infrared Spectroscopy and Electroencephalography. Clin Neurophysiol. 2021;132(7):1636–46.

19. Cooper RJ, Yucel M, Gagnon L, Suzuki N, Tanaka N, Reinsberger C, et al. Combining and optimizing NIRS and EEG to study interictal epileptic discharges. Biomed Opt 3-d Imaging. 2012;BSu2A.5.

20. Dehaes M, Cheng HH, Buckley EM, Lin PY, Ferradal S, Williams K, et al. Perioperative cerebral hemodynamics and oxygen metabolism in neonates with single-ventricle physiology. Biomed Opt Express. 2015;6:4749–67.

21. Durduran T, Zhou C, Buckley EM, Kim MN, Yu G, Choe R, et al. Optical measurement of cerebral hemodynamics and oxygen metabolism in neonates with congenital heart defects. J Biomed Opt. 2010;15:37004.

22. Durduran T, Choe R, Baker WB, Yodh AG. Diffuse optics for tissue monitoring and tomography. Rep Prog Phys. 2010;73(7):076701.

23. Boas DA, Yodh AG. Spatially varying dynamical properties of turbid media probed with diffusing temporal light correlation. J Opt Soc Am. 1997;14(1):192.

24. Durduran T, Yu G, Burnett MG, Detre JA, Greenberg JH, Wang J, et al. Diffuse optical measurement of blood flow, blood oxygenation, and metabolism in a human brain during sensorimotor cortex activation. Opt Lett. 2004;29(15):1766.

25. Durduran T, Yodh AG. Diffuse correlation spectroscopy for non-invasive, micro-vascular cerebral blood flow measurement. Neuroimage. 2014;85 Pt 1:51–63.

26. Durduran T, Zhou C, Edlow BL, Yu G, Choe R, Kim MN, et al. Transcranial optical monitoring of cerebrovascular hemodynamics in acute stroke patients. Opt Express. 2009;17(5):3884.

27. Shang Y, Cheng R, Dong L, Ryan SJ, Saha SP, Yu G. Cerebral monitoring during carotid endarterectomy using near-infrared diffuse optical spectroscopies and electroencephalogram. Phys Med Biol. 2011;56:3015–32.

28. Blume WT, Ferguson GG, McNeill DK. Significance of EEG changes at carotid endarterectomy. Stroke. 2018;17(5):891–7.

29. Klosek SK, Rungruang T. Topography of carotid bifurcation: considerations for neck examination. Surg Radiol Anat. 2008;30(5):383–7.

30. Boron WF, Boulpaep EL. Medical Physiology. Elsevier Health Sciences, 2016.

31. Hartkamp MJ, Grond J van der, Everdingen KJ van, Hillen B, Mali WPTM. Circle of Willis Collateral Flow Investigated by Magnetic Resonance Angiography. Stroke. 1999;30(12):2671–8.

32. North American Symptomatic Carotid Endarterectomy Trial Collaborators (NASCET). Beneficial Effect of Carotid Endarterectomy in Symptomatic Patients with High-Grade Carotid Stenosis. New Engl J Medicine. 1991 Aug 15;325(7):445–53.

33. Grotta JC. Clinical practice. Carotid stenosis. N Engl J Med. 2013;369:1143–50.

34. Carotid Endarterectomy. Available online: https://surgery.ucsf.edu/conditions--procedures/carotid-endarterectomy.aspx (accessed on 3 October 2022).

35. Medical Gallery of Blausen Medical 2014. Wikijournal Medicine. 2014;1(2). Available online: https://en.wikiversity.org/wiki/WikiJournal_of_Medicine/Medical_gallery_of_Blausen_Medical_2014 (accessed on 3 October 2022).

36. Hayes PD, Vainas T, Hartley S, Thompson MM, London NJM, Bell PRF, et al. The Pruitt-Inahara shunt maintains mean middle cerebral artery velocities within 10% of preoperative values during carotid endarterectomy. J Vasc Surg. 2000;32(2):299–306.

37. Moritz S, Kasprzak P, Arlt M, Taeger K, Metz C. Accuracy of Cerebral Monitoring in Detecting Cerebral Ischemia during Carotid Endarterectomy. Anesthesiology. 2007;107(4):563–9.

38. Haupt WF, Horsch S. Evoked potential monitoring in carotid surgery: A review of 994 cases. Neurology. 1992;42(4):835–835.

39. Kearse Jr LA, Brown EN, McPeck K. Somatosensory evoked potentials sensitivity relative to electroencephalography for cerebral ischemia during carotid endarterectomy. Stroke. 2018;23(4):498–505.

40. Belardi P, Lucertini G, Ermirio D. Stump pressure and transcranial Doppler for predicting shunting in carotid endarterectomy. Eur J Vasc Endovasc. 2003;25(2):164–7.

41. Harada RN, Comerota AJ, Good GM, Hashemi HA, Hulihan JF. Stump pressure, electroencephalographic changes, and the contralateral carotid artery: Another look at selective shunting. Am J Surg. 1995;170(2):148–53.

42. McKay RD, Sundt TM, Michenfelder JD, Gronert GA, Messick JM, Sharbrough FW, et al. Internal Carotid Artery Stump Pressure and Cerebral Blood Flow during Carotid Endarterectomy. Anesthesiology. 1976;45(4):390–9.

43. Spencer MP, Thomas GI, Nicholls SC, Sauvage LR. Detection of middle cerebral artery emboli during carotid endarterectomy using transcranial Doppler ultrasonography. Stroke. 1990;21:415–23.

44. Edlow BL, Kim MN, Durduran T, Zhou C, Putt ME, Yodh AG, et al. The effects of healthy aging on cerebral hemodynamic responses to posture change. Physiol Meas. 2010;31(4):477–95.

45. Pennekamp CWA, Bots ML, Kappelle LJ, Moll FL, Borst GJ de. The Value of Near-Infrared Spectroscopy Measured Cerebral Oximetry During Carotid Endarterectomy in Perioperative Stroke Prevention. A Review. Eur J Vasc Endovasc. 2009;38(5):539–45.

46. Chung F, Mezei G, Tong D. Pre-existing medical conditions as predictors of adverse events in day-case surgery. Bja Br J Anaesth. 1999;83(2):262–70.

47. Forrest JB, Rehder K, Cahalan MK, Goldsmith CH. Multicenter Study of General Anesthesia III. Predictors of Severe Perioperative Adverse Outcomes. Anesthesiology. 1992;76(1):3–15.

48. Holmström A, Åkeson J. Sevoflurane induces less cerebral vasodilation than isoflurane at the same A-line® autoregressive index level. Acta Anaesth Scand. 2005;49(1):16–22.

49. Kaisti KK, Metsähonkala L, Teräs M, Oikonen V, Aalto S, Jääskeläinen S, et al. Effects of Surgical Levels of Propofol and Sevoflurane Anesthesia on Cerebral Blood Flow in Healthy Subjects Studied with Positron Emission Tomography. Anesthesiology. 2002;96(6):1358–70.

50. Hans P, Bonhomme V. Why we still use intravenous drugs as the basic regimen for neurosurgical anaesthesia. Curr Opin Anaesthesiol. 2006;19(5):498–503.

51. Reinhard M, Roth M, Muller T, Guschlbauer B, Timmer J, Czosnyka M, et al. Effect of carotid endarterectomy or stenting on impairment of dynamic cerebral autoregulation. Stroke. 2004;35:1381–7.

52. Nouraei SAR, Al-Rawi PG, Sigaudo-Roussel D, Giussani DA, Gaunt ME. Carotid endarterectomy impairs blood pressure homeostasis by reducing the physiologic baroreflex reserve. J Vasc Surg. 2005;41(4):631–7.

53. Sigaudo-Roussel D, Evans DH, Naylor AR, Panerai RB, London NL, Bell P, et al. Deterioration in carotid baroreflex during carotid endarterectomy. J Vasc Surg. 2002;36(4):793–8.

54. Yakhou L, Constant I, Merle JC, Laude D, Becquemin JP, Duvaldestin P. Noninvasive investigation of autonomic activity after carotid stenting or carotid endarterectomy. J Vasc Surg. 2006;44(3):472–9.

55. Timmers HJLM, Buskens FGM, Wieling W, Karemaker JM, Lenders JWM. Long-term effects of unilateral carotid endarterectomy on arterial baroreflex function. Clin Auton Res. 2004;14(2):72–9.

56. Bigio IJ, Fantini S. Quantitative biomedical optics: theory, methods, and applications. Vol. 1 Ed. New York, NY: Cambridge University Press.; 2016.

57. Jacques SL. Optical properties of biological tissues: a review. Phys Med Biol. 2013;58(11):R37–61.

58. Sassaroli A, Fantini S. Comment on the modified Beer–Lambert law for scattering media. Phys Medicine Biology. 2004;49(14):N255–7.

59. Prahl S. Tabulated molar extinction coefficient for hemoglobin in water. Available online: http://omlc.ogi.edu/spectra/hemoglobin/summary.html (accessed on 3 October 2022).

60. Buckley EM, Cook NM, Durduran T, Kim MN, Zhou C, Choe R, et al. Cerebral hemodynamics in preterm infants during positional intervention measured with diffuse correlation spectroscopy and transcranial Doppler ultrasound. Opt Express. 2009;17(15):12571.

61. Roche-Labarbe N, Carp SA, Surova A, Patel M, Boas DA, Grant PE, et al. Noninvasive optical measures of CBV, StO(2), CBF index, and rCMRO(2) in human premature neonates' brains in the first six weeks of life. Human brain mapping. 2010;31:341–52.

62. Bonner R, Nossal R. Model for laser Doppler measurements of blood flow in tissue. Appl Optics. 1981;20(12):2097.

63. Sutin J, Zimmerman B, Tyulmankov D, Tamborini D, Wu KC, Selb J, et al. Time-domain diffuse correlation spectroscopy. Optica. 2016;3:1006–13.

64. Hueber DM, Franceschini MA, Redes N, Farzam P, Carp SA. Combined multi-distance frequency domain and diffuse correlation spectroscopy system with simultaneous data acquisition and real-time analysis. Biomed Opt Express. 2017;8(9):3993–4006.

65. Lemieux PA, Durian DJ. Investigating non-Gaussian scattering processes by using nth -order intensity correlation functions. J Opt Soc Am. 1999;16(7):1651.

66. Milej D, He L, Abdalmalak A, Baker WB, Anazodo UC, Diop M, et al. Quantification of cerebral blood flow in adults by contrast-enhanced near-infrared spectroscopy: Validation against MRI. J Cereb Blood Flow Metab. 2020;40:1672–84.

67. Carp SA, Dai GP, Boas DA, Franceschini MA, Kim YR. Validation of diffuse correlation spectroscopy measurements of rodent cerebral blood flow with simultaneous arterial spin labeling MRI; towards MRI-optical continuous cerebral metabolic monitoring. Biomed Opt Express. 2010;1(2):553–65.

68. Zhou C, Eucker SA, Durduran T, Yu G, Ralston J, Friess SH, et al. Diffuse optical monitoring of hemodynamic changes in piglet brain with closed head injury. J Biomed Opt. 2009;14:34015.

69. Giovannella M, Andresen B, Andersen JB, El-Mahdaoui S, Contini D, Spinelli L, et al. Validation of diffuse correlation spectroscopy against 15O-water PET for regional cerebral blood flow measurement in neonatal piglets. J Cereb Blood Flow Metabolism. 2019;40(10):2055–65.

70. Ferradal SL, Yuki K, Vyas R, Ha CG, Yi F, Stopp C, et al. Non-invasive Assessment of Cerebral Blood Flow and Oxygen Metabolism in Neonates during Hypothermic Cardiopulmonary Bypass: Feasibility and Clinical Implications. Sci Rep. 2017;7:44117.

71. Busch DR, Rusin CG, Miller-Hance W, Kibler K, Baker WB, Heinle JS, et al. Continuous cerebral hemodynamic measurement during deep hypothermic circulatory arrest. Biomed Opt Express. 2016;7:3461–70.

72. Jain V, Buckley EM, Licht DJ, Lynch JM, Schwab PJ, Naim MY, et al. Cerebral Oxygen Metabolism in Neonates with Congenital Heart Disease Quantified by MRI and Optics. J Cereb Blood Flow Metabolism. 2013;34(3):380–8.

73. Baker WB, Balu R, He L, Kavuri VC, Busch DR, Amendolia O, et al. Continuous non-invasive optical monitoring of cerebral blood flow and oxidative metabolism after acute brain injury. J Cereb Blood Flow Metab. 2019;39:1469–85.

74. Selb J, Wu KC, Sutin J, Lin PI, Farzam P, Bechek S, et al. Prolonged monitoring of cerebral blood flow and autoregulation with diffuse correlation spectroscopy in neurocritical care patients. Neurophotonics. 2018;5:45005.

75. Sunwoo J, Zavriyev AI, Kaya K, Martin A, Munster C, Steele T, et al. Diffuse correlation spectroscopy blood flow monitoring for intraventricular hemorrhage vulnerability in extremely low gestational age newborns. Sci Rep. 2022;12(1):12798.

76. Ayaz H, Baker WB, Blaney G, Boas DA, Bortfeld H, Brady K, et al. Optical imaging and spectroscopy for the study of the human brain: status report. Proc Spie. 2022;9(S2):S24001–S24001.

77. Selb JJ, Boas DA, Chan ST, Evans KC, Buckley EM, Carp SA. Sensitivity of near-infrared spectroscopy and diffuse correlation spectroscopy to brain hemodynamics: simulations and experimental findings during hypercapnia. Neurophotonics. 2014;1:15005.

78. Carp SA, Tamborini D, Mazumder D, Wu KC (Tony), Robinson MR, Stephens KA, et al. Diffuse correlation spectroscopy measurements of blood flow using 1064 nm light. J Biomed Opt. 2020;25(9):097003–097003.

79. Wolthuis R, Aken M van, Fountas K, Jr JSR, Bruining HA, Puppels GJ. Determination of water concentration in brain tissue by Raman spectroscopy. Analytical chemistry. 2001;73:3915–20.

80. Stoneham MD, Stamou D, Mason J. Regional anaesthesia for carotid endarterectomy. Bja Br J Anaesth. 2015;114(3):372–83.

81. Friedell ML, Clark JM, Graham DA, Isley MR, Zhang XF. Cerebral oximetry does not correlate with electroencephalography and somatosensory evoked potentials in determining the need for shunting during carotid endarterectomy. Journal of vascular surgery. 2008;48:601–6.

82. Grubhofer G, Plöchl W, Skolka M, Czerny M, Ehrlich M, Lassnigg A. Comparing Doppler ultrasonography and cerebral oximetry as indicators for shunting in carotid endarterectomy. Anesthesia & Analgesia. 2000;91:1339–44.

83. Samra SK, Dy EA, Welch K, Dorje P, Zelenock GB, Stanley JC. Evaluation of a cerebral oximeter as a monitor of cerebral ischemia during carotid endarterectomy. The Journal of the American Society of Anesthesiologists. 2000;93:964–70.

84. Spanos K, Nana P, Kouvelos G, Batzalexis K, Matsagkas MM, Giannoukas AD. Completion imaging techniques and their clinical role after carotid endarterectomy: Systematic review of the literature. Vascular. 2020;28:794–807.

85. Matsumoto S, Nakahara I, Higashi T, Iwamuro Y, Watanabe Y, Takahashi K, et al. Near-infrared spectroscopy in carotid artery stenting predicts cerebral hyperperfusion syndrome. Neurology. 2009;72(17):1512–8.

86. Rigamonti A, Scandroglio M, Minicucci F, Magrin S, Carozzo A, Casati A. A clinical evaluation of near-infrared cerebral oximetry in the awake patient to monitor cerebral perfusion during carotid endarterectomy. Journal of clinical anesthesia. 2005;17:426–30.

87. Pugliese F, Ruberto F, Tosi A, Martelli S, Bruno K, Summonti D, et al. Regional cerebral saturation versus transcranial Doppler during carotid endarterectomy under regional anaesthesia. European Journal of Anaesthesiology| EJA. 2009;26:643–7.

88. Pedrini L, Magnoni F, Sensi L, Pisano E, Ballestrazzi MS, Cirelli MR, et al. Is near-infrared spectroscopy a reliable method to evaluate clamping ischemia during carotid surgery? Stroke Research and Treatment. 2012;2012.

89. Mille T, Tachimiri ME, Klersy C, Ticozzelli G, Bellinzona G, Blangetti I, et al. Near Infrared Spectroscopy Monitoring During Carotid Endarterectomy: Which Threshold Value is Critical? Eur J Vasc Endovasc. 2004;27(6):646–50.

90. Ritter J, Green D, Slim H, Tiwari A, Brown J, Rashid H. The role of cerebral oximetry in combination with awake testing in patients undergoing carotid endarterectomy under local anaesthesia. European Journal of Vascular and Endovascular Surgery. 2011;41:599–605.

91. Yu B, Peng Y, Qiao H, Liu B, Wang M, Yang X, et al. The Application of Regional Cerebral Oxygenation Monitoring in the Prediction of Cerebral Hypoperfusion During Carotid Endarterectomy. J Neurosurg Anesth. 2022;34(1):29–34.

92. Pinkerton JA. EEG as a Criterion for Shunt Need in Carotid Endarterectomy. Ann Vasc Surg. 2002;16(6):756–61.

93. Ozana N, Zavriyev AI, Mazumder D, Robinson M, Kaya K, Blackwell M, et al. Superconducting nanowire single-photon sensing of cerebral blood flow. Proc Spie. 2021;8(3):035006–035006.

94. Kaya K, Zavriyev AI, Sunwoo J, Simon MV, Pierce ET, Franceschini MA. Detection of cerebral blood flow and hemoglobin oxygenation using diffuse correlation spectroscopy and frequency-domain near-infrared spectroscopy during carotid endarterectomy. Proc SPIE. 2021;11629:116291A– 4.

95. Silbert BS, Kluger R, Cronin KD, Koumoundouros E. The Processed Electroencephalogram May Not Detect Neurologic Ischemia during Carotid Endarterectomy. Anesthesiology. 1989;70(2):356–7.

96. Engelhard K, Werner C. Inhalational or intravenous anesthetics for craniotomies? Pro inhalational. Curr Opin Anaesthesiol. 2006;19(5):504–8.

97. McCulloch TJ, Thompson CL, Turner MJ. A Randomized Crossover Comparison of the Effects of Propofol and Sevoflurane on Cerebral Hemodynamics during Carotid Endarterectomy. Anesthesiology. 2007;106(1):56–64.

98. Godet G, Reina M, Raux M, Amour J, Castro VD, Coriat P. Anaesthesia for carotid endarterectomy: comparison of hypnotic- and opioid-based techniques†. Bja Br J Anaesth. 2004;92(3):329–34.

99. Zhan X, Fahlman CS, Bickler PE. Isoflurane Neuroprotection in Rat Hippocampal Slices Decreases with Aging. Anesthesiology. 2006;104(5):995–1003.

100. Feiner JR, Bickler PE, Estrada S, Donohoe PH, Fahlman CS, Schuyler JA. Mild Hypothermia, but Not Propofol, Is Neuroprotective in Organotypic Hippocampal Cultures. Anesthesia Analgesia. 2005;100(1):215–25.

101. Engelhard K, Werner C, Eberspächer E, Pape M, Stegemann U, Kellermann K, et al. Influence of Propofol on Neuronal Damage and Apoptotic Factors after Incomplete Cerebral Ischemia and Reperfusion in Rats. Anesthesiology. 2004;101(4):912–7.

102. Payne RS, Akca O, Roewer N, Schurr A, Kehl F. Sevoflurane-induced preconditioning protects against cerebral ischemic neuronal damage in rats. Brain Res. 2005;1034(1–2):147–52.

103. Conti A, Iacopino DG, Fodale V, Micalizzi S, Penna O, Santamaria LB. Cerebral haemodynamic changes during propofol–remifentanil or sevoflurane anaesthesia: transcranial Doppler study under bispectral index monitoring. Bja Br J Anaesth. 2006;97(3):333–9.

8. APPENDIX

APPENDIX 1: Massachusetts General Hospital and Mass General Brigham (f/k/a Partners HealthCare) Institutional Research Board

PARTNERS HEALTHCARE
FOUNDED BY BRIGHAM AND WOMEN'S HOSPITAL AND MASSACHUSETTS GENERAL HOSPITAL

Partners Human Research Committee
116 Huntington Avenue, Suite 1002
Boston, MA 02116
Tel: (617) 424-4100
Fax: (617) 424-4199

Initial Review: Notification of IRB Approval/Activation
Protocol #: 2015P002669/MGH

Title of Protocol:	Optical monitoring of cerebral blood flow and metabolism during carotid endarterectomy

IRB Approval Date:	3/10/2016
Approval Activation Date:	3/16/2016
IRB Expiration Date:	3/10/2017

APPENDIX 2: Thesis Originality Report

turnitin

Dijital Makbuz

Bu makbuz ödevinizin Turnitin'e ulaştığını bildirmektedir. Gönderiminize dair bilgiler şöyledir:

Gönderinizin ilk sayfası aşağıda gönderilmektedir.

Gönderen:	Kutlu Kaya
Ödev başlığı:	Tez Deneme1
Gönderi Başlığı:	Doktora Tez Son
Dosya adı:	Dr_Dissertation_copy.pdf
Dosya boyutu:	4.62M
Sayfa sayısı:	65
Kelime sayısı:	16,580
Karakter sayısı:	87,019
Gönderim Tarihi:	03-Eki-2022 01:29ÖS (UTC+0300)
Gönderim Numarası:	1915300347

T.C.
REPUBLIC OF TURKEY
HACETTEPE UNIVERSITY
GRADUATE SCHOOL OF HEALTH SCIENCES

OPTICAL MONITORING OF CEREBRAL BLOOD FLOW AND METABOLISM DURING CAROTID ENDARTERECTOMY

Kutlu KAYA, M.S.

Program of Physiology
DOCTOR OF PHILOSOPHY DISSERTATION

ANKARA
2022

APPENDIX 2 (*Cont.*): Thesis Originality Report

Tezin Tam Başlığı: Optical Monitoring of Cerebral Blood Flow and Metabolism During Carotid Endarterectomy
Öğrenci Ad Soyad: Kutlu Kaya
Toplam Sayfa Sayısı: 74

ORİJİNALLİK RAPORU

%7	%4	%6	%1
BENZERLİK ENDEKSİ	İNTERNET KAYNAKLARI	YAYINLAR	ÖĞRENCİ ÖDEVLERİ

BİRİNCİL KAYNAKLAR

1	D. A. Boas, A. G. Yodh. "Spatially varying dynamical properties of turbid media probed with diffusing temporal light correlation", Journal of the Optical Society of America A, 1997 Yayın	<%1
2	dokumen.pub İnternet Kaynağı	<%1
3	www.spie.org İnternet Kaynağı	<%1
4	"Anesthesia for Carotid Endarterectomy", Neuroanesthesia and Cerebrospinal Protection, 2015. Yayın	<%1
5	academic.oup.com İnternet Kaynağı	<%1
6	www.nature.com İnternet Kaynağı	<%1
7	core.ac.uk İnternet Kaynağı	<%1

9. CURRICULUM VITAE